Research papers

Desiccation of the Transboundary Hamun Lakes between Iran and Afghanistan in Response to Hyro-climatic Droughts and Anthropogenic Activities

Mahdi Akbari[a,*], Ali Mirchi[b], Amin Roozbahani[c], Abror Gafurov[d], Bjørn Kløve[a] and Ali Torabi Haghighi[a]

a Water, Energy and Environmental Engineering Research Unit, Faculty of Technology, University of Oulu, Finland

b Department of Biosystems and Agricultural Engineering Oklahoma State University, Stillwater, USA

c Nimab-tose Consulting Engineering Company, Tehran, Iran

d GFZ German Research Centre for Geosciences, Section 5.4 Hydrology, Potsdam, Germany

**Corresponding author: mahdi.akbari@oulu.fi[*]*

The paper is a non-peer reviewed preprint submitted to EarthArXiv. Also, this manuscript has been submitted in **Great Lake Research Journal** for peer review. Please feel free to contact corresponding author for any question or feedback.

---

[*] Permanent address:

University of Oulu

P.O. BOX 8000

FI-90014

Abstract

This paper investigates the hydro-climatic reasons behind the desiccation of the Hamun Lakes in the Iran-Afghanistan border. We analyzed changes in the flow of the Hirmand River (90 percent of the total inflow to the lakes) at the international border, and precipitation over this river's sub-basin during 1960-2016 by calculating standardized indices for precipitation (SPI) and discharge (SDI). We applied Normalized Difference Spectral Indices using satellite images from 1987-2021 to observe monthly areal change of the lakes. The results show that the major cause of desiccation is upstream water regulation which severely reduced the Hirmand River inflow delivery to the lakes. Also, recently constructed reservoirs, near the lakes, compounded the effect of upstream water regulation to aggravate the situation. There is a discernible shift in the relation between the Hirmand River flow at the border and upstream precipitation before and after 2004. In 1960-2003, high Hirmand River inflows were expected due to high precipitation, while the flow declined after 2004 despite large amounts of upstream precipitation. Although a long period of drought from 1998-2004 decreased the lakes' area, the lake system is primarily falling victim to anthropogenic flow reduction in the transboundary basin. Increased regulation of flows and use of water for irrigation in Afghanistan and Iran underscores the necessity of bilateral dialogues between the two countries to consider environmental flow of the lakes. The lakes' shrinkage places socio-economic stress on an already-vulnerable region with public health implications as the exposed lake beds turn into major sources of dust storms.

Key words

Standardized Precipitation Index (SPI), Standardized Discharge Index (SDI), Normalized Difference Spectral Indices (NDSIs), Water Management, Lake Desiccation, Aral-Sea Syndrome

1. Introduction

The Hamun Lakes are the largest (> 8000 km^2) fresh body of water in the Iran plateau, which nearly desiccated after 2005 (Pekel et al., 2016). Climatic variation is an important driver of the change of water-land in large scales (Akbari et al., 2020; Ehsani et al., 2020; Haghighi and Kløve, 2015; Milly and Dunne, 2016; Rahimi et al., 2020). However, there is growing concern that human activities are a substantial, sometimes dominant reason for decline of water bodies, triggering a host of environmental and economic consequences (AghaKouchak et al., 2015; Chaudhari et al., 2018; Haghighi et al., 2020; Khazaei et al., 2019; Zaki et al., 2020). For example, the dry-up of water bodies due to anthropogenic effects (e.g. agricultural activities), i.e. so-called Aral-Sea desiccation syndrome (AghaKouchak et al., 2015), have been documented in Central Asia (Micklin, 1988) and northwestern Iran (Akbari et al., 2019; Alborzi et al., 2018).

The Hamun Lakes are crucial for the economy and environment of the surrounding area (Rashki et al., 2012). The main rivers that sustain the lakes originate in Afghanistan. Hirmand (or Helmand) River, the most important river feeding the lake system and a crucial water source for Afghan and Iranian farmers (Ahlers et al., 2014), is shared based on the bilateral treaty in 1973 (Helmand Commission, 1973). The 1973 agreement guarantees to supply Iran with an average 22 m^3/s plus 4 m^3/s (for "goodwill and brotherly relations"), providing a basis for monthly allocation of the Hirmand River flow to Iran. Thus, Iran's annual share of Hirmand River flow is about 0.82 km^3 (Figure 1-f). Monthly flow deliveries are based on "normal water years" (Article II), which is defined (Article I) as a year with total flows upstream of Kajaki Dam being more than 5.661 km^3 between 1 October and the following 30 September. Therefore, this treaty is flexible in dry years, i.e., water deliveries are adjusted proportionally to deviations from predefined normal years (Article IV). Also, Afghanistan must supply water of a quality that can be treated, if necessary, for irrigation and domestic uses (Art.

61 VI). The 1973 treaty does not address the environmental water right of the Hamun Lakes; thus, Iran
62 utilizes 0.82 km^3 of water considered in the treaty for potable and agricultural uses. Iran Department
63 of Environment (DOE), estimated that annually 7.67 km^3 environmental flow is needed for ecological
64 restoration of the lakes (DOE, 2014). Other studies (Amini et al., 2021; Thomas and Varzi, 2015),
65 confirmed the inadequacies of the 1973 treaty for sustainable transboundary water resources
66 management in which environmental flow right of the lakes is considered. From 2002 to 2021,
67 agricultural water consumption of the basin has increased from 2 to over 6 km^3 (Akbari and Haghighi,
68 2022). Recent agricultural development and water resources management in the region is giving rise
69 to classic upstream-downstream water tensions that adversely affect the socio-economically vulnerable
70 residents in the border region, including the Sistan and Baluchistan province of Iran (Ahlers et al.,
71 2014).

72 The Hamun Lakes are a major dust source in southwest Asia (Goudie and Middleton, 2006) due
73 to strong winds (known as "120-day wind") in the region (Hossenzadeh, 1997). The communities
74 around the lakes are affected by post-desiccation dust storms (Rashki et al., 2012). Furthermore, the
75 sand and dust storms affect the whole Sistan region in Iran, southwest Afghanistan, and Pakistan (Alam
76 et al., 2011; Goudie and Middleton, 2000; Rashki et al., 2012). Zaranj City (Figure 1-b) is the largest
77 population center (~160,000 people) in Afghanistan close to the lakes (Afganistan Ministry of Urban
78 Development Affairs, 2015). The population in urban areas is larger on the Iranian side where Zahedan
79 (~590,000 people) and Zabol (~134,000 people) are located (Statistical Center of Iran, 2016). In 2012
80 Zabol had the most polluted air in the world. In this year, the concentration of mean annual particulate
81 matter with 10 and 2.5 micrometers or less in diameter (PM_{10} and $PM_{2.5}$) in Zabol reached 527 and
82 217 $\mu g/m^3$, respectively (WHO, 2016), far exceeding WHO's safe concentration thresholds for PM_{10}
83 (20 $\mu g/m^3$) and $PM_{2.5}$ (10 $\mu g/m^3$). Consequently, respiratory diseases are a common public health

hazard in Zabol with medical costs exceeding USD 166.7 Million U.S. during 1999–2004 (Miri et al., 2007).

As mounting concerns about the drying of the Hamun Lakes give rise to potential water conflicts in this transboundary basin (Dehgan et al., 2014; Mianabadi et al., 2021), it is necessary to evaluate whether the shrinkage is governed by climatic conditions or if the problem has emerged as a result of anthropogenic water regulation. This understanding is an important precursor for effective plans to protect the socio-ecological system based on binational cooperation between Iran and Afghanistan. To this end, we investigate the climatic and hydrological drivers of the desiccation of the Hamun Lakes alongside a shift in water management paradigm that has marginalized environmental flows. Our analysis covers water resources management on both sides of the border, namely upstream dams in Afghanistan, as well as water regulation of the Hirmand River in Iran by constructing reservoirs in the Sistan region. We study hydrological and meteorological droughts in the Hirmand River sub-basin from 1960-2016 to characterize the Hirmand River flow alteration at the international border. Notwithstanding the hydro political complexity of the transboundary region, our hydro-climatological investigation of the connected lakes provides useful insights into the mechanism of desiccation and potential reasons behind the decline of the connected lakes.

2. Materials and Methods

2.1. Study area

Hamun Lakes are in the Iran-Afghanistan border zone in the Sistan region (Figure 1-a) within the transboundary Helmand Basin. The lake system is a Ramsar site (The Convention on Wetlands, 1975). Helmand Basin (area: ~350,000 km^2) is the largest basin in Afghanistan, covering 43% of the country. Most of this transboundary basin (~80%) is in Afghanistan, less than 5% in Pakistan and the rest in

Iran (Figure 1-a). Hirmand River sub-basin is a part of the Helmand Basin as shown in Figure 1-a. As the terminal point of an endorheic basin, the Hamun Lake system is primarily fed by rivers that originate in the Hindu Kush mountain range. Other major tributaries besides the Hirmand (or Helmand) River (mean annual flow: ~ 6 km^3) include Farah, Khash, Khospas and Adraskan (or Harut) (Figure 1-a). Total inflow from Farah, Khash, Khospas, Adraskan and other minor tributaries is 0.54 km^3 (DOE, 2014). Thus, over 90 percent of total inflow to the lakes is provided by the Hirmand River. Two of the largest dams in Afghanistan, namely Kajaki (capacity 2.5 km^3) and Arghandab (or Dahla, capacity 0.5 km^3), were built in this basin in 1952 (Lehner et al., 2011). Based on data from 1960-1980, the maximum monthly inflow to these dams occurred in April, averaging about 1.5 and 0.6 km^3, respectively (Williams-Sether, 2008). Also, the Kamal-Khan Dam with current capacity equal to 0.05 km^3 is the largest hydraulic structure on the Hirmand River after the Kajaki Dam (Figure 1-a). Construction of this dam began in 1996 but it was halted due to the civil war in Afghanistan. The project recommenced in 2011 and phase II was completed in 2015. Work on phase III began in 2017 and the dam went into operation in 2021. The objective has been to provide water for irrigation of agricultural land in Afghanistan, flood protection, drinking water and generation of 9 MW of electricity.

According to the Köppen-Geiger climate classification (Kottek et al., 2006), the Helmand Basin's climate varies from highlands to downstream areas, ranging from snow climate with dry summers (Ds) in the Hindu Kush mountain range to warm temperate climate with dry summer (Cs) in the foothills of the Hindu Kush mountains and steppe climate (BS) and desert climate (BW) downstream of Kajaki and Arghandab Dams (Appendix A, Figure S 1-a). Based on the Global Precipitation Climatology Centre (GPCC) dataset (Schneider et al., 2011), the basin's annual precipitation varies from more than 1200 mm in the Hindu Kush highlands to less than 60 mm in the lowlands near the Hamun Lakes (see Appendix B). "120-Day winds" are frequent and intensive, especially during the summer (Goudie and

130 Middleton, 2000), and their speed reaches over 100 km/s (Meteorological Department of Sistan and
131 Baluchestan, 2020).

132 The Hamun Lakes consist of three connected Lakes above Shile Canal (Figure 1-b), namely
133 Hamun-i Puzak ($max\ area = 1{,}500$ km^2), Hamun-i Saburi ($max\ area = 1{,}500$ km^2) and Hamun-i
134 Hirmand ($max\ area = 2{,}000$ km^2), and a deeper terminal lake named Gaud-i Zirreh ($max\ area =$
135 $3{,}000$ km^2) (Figure 1-a). Hamun-i Puzak with entrance elevation of 480 meter (m) above mean sea
136 level (AMSL) at the outlet of the Paryan River (Figure 1-c) is the first lake in this cascading lake
137 system. The lowest bed elevation at Hamun-i Puzak is 475.5 m AMSL, and excess flow after filling
138 this lake spills into Hamun-i Saburi at 477 meter AMSL, which discharges into the downstream
139 Hamun-i Hirmand at 474.5 m AMSL (Figure 1-c). Finally, the last lake is Gaud-i Zirreh, which is fed
140 by Shile Canal in the south of Hamun-i Hirmand (Figure 1-b). Mean depth of the first three lakes
141 (Hamun-i Puzak, Hamun-i Saburi and Hamun-i Hirmand) is 1 meters (ModaresiRad et al., 2022), while
142 Gaud-i Zirreh is the deepest lake with a mean depth of 10 m. Mean annual flow for Shile Canal (inflow
143 to Gaud-i Zirreh) at Pol-Shile station is about 3 km^3 (1990-1998), which decreased to almost zero after
144 1999 (HIWRI, 2017).

145 Hirmand River bifurcates into two rivers after entering Iran: Sistan and Paryan Rivers (Figure 1-
146 d). Paryan River flows to Hamun-i Puzak, and Sistan River finally ends in Hamun-i Saburi and Hamun-
147 i Hirmand (Figure 1-b). Based on long-term flow data (gauges shown in Figure 1-d), 47% of the total
148 inflow of the Hirmand River is observed in Choto gauge on the Paryan River while the rest is recorded
149 by Kahak gauge on the Sistan River (MoE, 2014). Some parts of the Sistan River flow were diverted
150 by Kahak diversion dam (Figure 1-d) to four reservoirs named Chah Nimeh Reservoirs (CNR1 through
151 4) through the Feeder Canal (shown as FC in Figure 1-d with $capacity = 600\ m^3/sec$). CNR1 (Cap:
152 0.220 km^3), CNR2 (Cap: 0.090 km^3), and CNR3 (0.320 km^3) were constructed in 1983. The last and

largest reservoir, i.e. CNR4 (Cap: 0.810 km^3) was commissioned in 2008 but initial filling began sooner (Absaran Consulting Company, 2015). The main purposes of CNRs in Iran are to meet agricultural (0.4 km^3/yr), domestic (0.11 km^3/yr), and industrial (0.03 km^3/yr) demands of the Sistan region based on the current status of the basin, totaling 0.54 km^3/yr (MoE, 2014). CNRs are connected, each spilling to the next at 480 m AMSL. Feeder Canal discharges into CNR1, and then into CNR2 until all CNRs are sequentially filled. When all CNRs are full, the overflow is directed to the Sistan River from the north of CNR1 and west of CNR4 by two canals known as Head Race (HR shown in Figure 1-d). Both HRs have been equipped with floodgate to regulate outflow. Near CNRs pan evaporation is reported to be 4,836 mm/yr and annual potential evaporation from water surface in the Sistan region is estimated to be 2585 mm (DOE, 2014). Also, the annual volume of actual evaporation from the CNRs water surface is 0.306 km^3 (MoE, 2014).

2.2. Data

The spatiotemporal scope of the study was determined based on data availability and predominant inflow into the lakes. We limited our investigation to Hirmand River sub-basin (Figure 1-a) for 1960-2016. The annual flow data from 1960 to 2016 for Choto and Kahak gauges on Sistan and Paryan Rivers next to the border on the Iranian side (Figure 1-d) were obtained from Iran Ministry of Eenergy (MoE, 2014). Also, USGS data-base (Williams-Sether, 2008) provides flow data for period 1955-1980 at gauges located in Afghanistan (Figure 1-a and Figure S1) .

We calculated annual precipitation and inflow based on the defined water year in the 1973 treaty (i.e., from the first of October to the end of following year September). Available rain gauge data in the study area in Afghanistan and Iran do not have good spatial and temporal coverage. Thus, we used widely-applied satellite-based rainfall products, namely GPCC (Schneider et al., 2011), PERSIANN-CDR (Ashouri et al., 2015) and TRMM-3B43 (Huffman et al., 2007). All of these products show high

amount of precipitation in the region in the 2010-2016 period (more detail in Appendix B). We utilized different sources of precipitation products to ensure that the increasing trend of precipitation is recorded by various data sources. A comprehensive evaluation of currently available precipitation datasets over Iran at monthly (44 datasets) and daily (34 datasets) time scales (Saemian et al., 2021) as well as European Centre for Medium-Range Weather Forecasts Reanalysis (ERA) precipitation product (Ghajarnia et al., 2021) have shown that the GPCC overall matches the rain gauges network records better than other products over eastern basins of Iran. Therefore, we used the GPCC to estimate precipitation over Hirmand River sub-basin from 1960-2016. Also, satellite images from MODIS and Landsat were used to monitor water bodies area change. Digital elevation model (DEM) data are from ALOS World 3D — 30m (AW3D30) (Tadono et al., 2016).

2.3. Methodology

2.3.1. Water body detection

The Normalized Difference Spectral Indices (NDSIs) are commonly used for surface water detection (Boschetti et al., 2014). Among different NDSIs, those using visible bands (such as red, green, etc.), near-infrared band and short wave near infrared band have been shown to outperform others (Boschetti et al., 2014). The Normalized Difference Vegetation Index (NDVI) and the Normalized Difference Water Index (NDWI) are two examples of this class of NDSIs, which facilitate water detection (Chipman and Lillesand, 2007; Ouma and Tateishi, 2006; Pekel et al., 2016; Rokni et al., 2014; Rouse Jr, 1973; Zaki et al., 2018). Both indices are based on normalized difference of bands in the electromagnetic spectrum and vary between -1.0 to 1.0:

$$NDWI = (NIR - SWIR)/(NIR + SWIR) \quad (1)$$

$$NDVI = (NIR - Red)/(NIR + Red) \quad (2)$$

196 where NIR, RED and SWIR are reflections in the near-infrared, red visible and short wave near
197 infrared.

198 Positive NDWI and negative NDVI values represent water. Specific thresholds are needed to
199 determine water surfaces from other land cover types. We have access to multispectral remotely sensed
200 products from different satellites, such as Sentinel, Landsat, and MODIS. We utilized MODIS images
201 available after year 2001 because daily temporal resolution of this product helps resolve the common
202 cloud cover issue by providing more images in each month. Furthermore, we used Landsat images
203 available for the study area from 1987-2001 to expand our temporal coverage. We used MODSI NDWI
204 and Landsat NDVI products due to their good quality (i.e., less noise) in the study region to determine
205 the monthly variation of the water bodies' area. Finally, $NDVI < 0.04$ and $NDWI > 0.17$ were
206 considered as water using Google Earth Engine Java Script API (Gorelick et al., 2017) (the source
207 code is provided in supplementary materials).

208 2.3.2. Hamun Lakes rate of desiccation

209 We quantified the monthly rate of desiccation (i.e., $d(area)\ /d(time)$) for Hamun Lakes when
210 they receive no inflow. The monthly flow of Hirmand River at the border was zero from March 1999
211 to August 2002, providing a suitable timeframe for the analysis. We used the monthly area of all
212 Hamun Lakes from Landsat and MODIS satellites during this period to estimate how fast Hamun
213 Lakes desiccate after the inflow is cut. Quantifying the rates of desiccation can show how fast each
214 lake desiccates. This rate is affected by the depth of each water body because evaporation is larger in
215 shallower lakes.

216 2.3.3. Sensitivity of the Hamun Lakes area to monthly inflow from Hirmand River

217 The relationship between Hirmand inflow and the lakes' area was investigated based on monthly
218 area and inflow of Hirmand River to Iran from Jan. 1987 to Aug. 2013, i.e., the period with available

monthly flow data. We defined three classes of monthly inflow: 1) inflow less than 0.5 km^3 (275 cases), 2) inflow between 0.5 and 1 km^3 (30 cases) and 3) inflow more than 1 km^3 (15 cases). We chose 0.5 km^3 as a threshold of runoff classes because this is approximately equal to the active capacity of CNR4 and water demand in the Sistan region. This approach allowed an investigation of how water demand and the new water regulation capacity of CNR4 affected the area of the lakes.

2.3.4. Drought Indices (SPI and SDI)

Using annual (Oct. to Sep.) precipitation and runoff, we calculated Standardized Precipitation Index (SPI) and Standardized Discharge Index (SDI). To analyze the temporal hydro-climatological status of the Hirmand River sub-basin, the trend, the variation, and the average value of rainfall and discharge were calculated. Temporal climate variability was characterized using SPI, which is designed to evaluate metrological drought (McKee, 1995) and has been widely used for evaluating climate variability (Hao et al., 2014; Irannezhad et al., 2015). SPI requires fitting a probability density function (McKee, 1995; Thom, 1966) to the frequency distribution of precipitation at a given station for a particular timescale (e.g. 3 months and 6 months). In this study, annual SPI was estimated as (Farahmand and AghaKouchak, 2015):

$$SPI = \emptyset^{-1}(p) \qquad 3$$

where $\emptyset$ is the standardized normal distribution function and p is the corresponding empirical probability when the precipitation in Hirmand River sub-basin is sorted in ascending order. Based on SPI, climate conditions can be divided into eight categories as classified in Table 1.

SDI is calculated using the same approach as SPI but using the recorded annual river flow of Hirmand River at the Iran-Afghanistan border instead of precipitation. SPI and SDI are used to describe various drought categories. Over time, increased water consumption typically occurs in the upstream part of many basins. Increasing upstream water withdrawal or land-use change which can significantly

alter river flow, and subsequently downstream water delivery. Comparison between SPI and SDI can reveal how the association between upstream precipitation and downstream flow is impacted by climatic or anthropogenic drivers in the long term (Shukla and Wood, 2008; Torabi Haghighi et al., 2020). Also, we compared results of SPI with Standardized Precipitation Evapotranspiration Index (SPEI) to consider the effect of evapotranspiration. It was found that SPI and SPEI are consistent in terms of categorizing years based on drought condition (more detail in Appendix D).

2.4. Limitations and data uncertainty

Lack of information and data is a major barrier for Afghanistan's engagement with riparian neighbors on transboundary issues. Since 1979, no hydrologic data has been published publically in this country (Ahlers et al. 2014; Williams-Sether 2008), increasing uncertainties. For example, an accurate estimation of the magnitude of discharge into the Hamun Lakes is not possible (MoE, 2015), primarily due to the lack of river flow data in Afghanistan, especially on the northern tributaries. Using the main river flow data is recommended in the literature to characterize the hydrologic conditions to the extent possible despite lack of data on other feeding tributaries (Akbari et al., 2020; Chen et al., 2017). We used flow data at the border available from Iran. However, the amount of water diversions from the Hirmand River between the border and the water bodies is not available. Additionally, due to lack of water level data for the lakes, the best thresholds to detect water by NDVI (< 0.04) and NDWI (> 0.17) were selected by comparing different thresholds' results with Pekel et al. (2016) study (more detail in Appendix E).

3. Results

3.1. Areal change of the lakes and CNRs in the Sistan region

The monthly area of CNRs (Figure 2-e to h) shows that these reservoirs did not experience complete desiccation in all operating years except at the beginning of the 2000s due to extremely dry conditions (Table 1). However, monthly area variation in Hamun Lakes is high. Sometimes the area approaches zero, i.e., complete desiccation (boxplot in Figure 2-a to d).The CNRs exhibited low variation in monthly average area in all years of operation (boxplots in Figure 2-e to h). Therefore, coefficients of variation for monthly areas are 8.4%, 8.8%, 3.8% and 26.4% for CNR1 to CNR4 respectively.

Monthly area of the Hamun Lakes (Figure 2-a to d) starts to decrease after April-May when inflow diminishes in the region (Figure 5-d). However, Gaud-i Zirreh has completely desiccated (Figure 2-d) because inflow to Shile Canal approached zero since 1999. The monthly areal change of this water body has different pattern than the other lakes (boxplot of Figure 2-d). CNR1, CNR2 and CNR3 also reached maximum area in April-May (boxplots in Figure 2-e to g) when Hirmand River deliveries to Iran increased (Figure 5-d). CNR4 is Iran's last man-made reservoir in the series, receiving overflow from CNR1, 2 and 3 when these reservoirs are filled in April-May by spring flow. Thus, the area of CNR4 starts to increase after April-May. Based on the falling limb of the boxplots in Figure 2-e to g, the area of CNR1, 2 and 3 decreased in October, November and December because of conveying water to CNR4 (i.e., the rising limb of the boxplot shown in Figure 2-h). This operation strategy prepares CNR1, CNR2 and CNR3 to capture inflow in April-May by lowering the water level in CNR1 to maximize the discharge of the Feeder Canal (Figure 1-d), which is why the area of CNR4 is the highest during this period.

After April-May, the lakes gradually decreased to less than 5% of maximum area due to low inflow (falling limb of monthly inflow hydrograph in Figure 5-d) and high evaporation rate in the desert climate. Based on available images from Landsat and MODIS satellites from 1987-2020 (Figure 2), after 1990, all the Hamun Lakes had a large area, indicating that the highest inflow of Hirmand River to Iran since 1960 occurred in 1990 (Figure 1-e). After the onset of a severe drought period in 1999 ($SDI = -1.5$) and 2000 ($SDI < -2$), shown in Figure 5-a, the annual maximum area of Hamun-i Puzak, Hamun-i Saburi did not change considerably, but the duration of complete desiccation was relatively longer compared to before the dry years in 1999-2000 (Figure 2-a and b). On the other hand, Hamun-i Hirmand almost dried up (lower maximum annual area and longer complete desiccation in Figure 2-c). Gaud-i Zirreh (depth: $\approx$10 m), which is more than 5 times deeper than the other lakes, is the only water body in this system that did not completely desiccate immediately after the severe drought of 1999-2000 and 2001-2002 (SDI close to -2).

3.2. Rate of desiccation of Hamun Lakes

In the beginning of March 1999, Hamun-i Hirmand was 950 km^2, i.e. half of the maximum area based on available satellite images since 1987. Hamun-i Hirmand dried up over the next eight months when inflow to Hamun Lakes was zero (Figure 3). The slope of the desiccation line was lower when the lake's area was between 950-700 km^2 compared with when the area ranged 700-0 km^2, which means the shrinkage process accelerates as the water body becomes smaller (Figure 3). Seventeen months after the lake's inflow was completely halted (started in March 1999), Hamun-i Puzak and Hamun-i Saburi dried up completely. The rates of desiccation (i.e., slope of the lines in Figure 3) for Hamun-i Puzak, Hamun-i Saburi, and Gaud-i Zirreh are steeper in the beginning. Gaud-i Zirreh is more resistant to inflow cut—Shile Canal inflow was zero after 1999—and its complete desiccation takes about 6 years (70 months) due to higher depth of this lake compared to others.

3.3. Water flow through Hamun Lakes

We chose the 1988-1991 period to demonstrate how Hamun Lakes fill up and connect to each other (Figure 4); since in this period the lakes change from almost completely dry to full as captured by satellite images. The year 1988 ($SDI = 0.7$) was a transition year from the 1983-1987 dry period ($SDI < 0$ except 1985 when $SDI = 0.2$) to a very wet year in 1989 ($SDI = 1.1$) and an extremely wet year in 1990 ($SDI > 2$).

In the first months of 1988 (mildly wet based on Table 1), the Hamun Lakes were nearly empty due to the preceding drought period. The water area in the Northern Hamun Lakes started to increase in January to May by inflow in the same month but Gaud-i Zirreh kept shrinking because the level of water in northern Hamuns were not enough to feed the Shile Canal (compare Figure 4, 1988-03 and 1988-05; also overflow between northern Hamuns is observable). All the Hamun Lakes shrank (Figure 4, compare 1998-05 and 1988-07) during May-November 1988 due to reduced inflow in May (to almost zero) and water loss to evaporation. Inflow in December 1988 and January 1989 raised the water area in the northern lakes (Figure 4, compare 1988-12 and 1989-02) immediately. A similar pattern is observed in 1989 (very wet year) when inflow was enough to reach Hamun-i Hirmand, although the Shile Canal and consequently Gaud-i Zirreh were not fed (Figure 4, 1989-04). In 1990 (extremely wet year), inflow was the highest since 1960 and Shile Canal delivery increased the water area in Gaud-i Zirreh (Figure 4, 1990-01). When inflow decreased in May 1990, the shallow lakes upstream of the Shile Canal, lost considerable area immediately. Expectedly, it took longer for deeper portions of the cascading lakes to desiccate in response to decreased inflow.

In March 1991 maximum recorded inflow (4.5 km^3) of the Hirmand River entered Iran. Maximum area for Hamun-i Puzak (1300 km^2) and Hamun-i Saburi (1500 km^2) was observed in this month but the maximum area of Hamun-i Hirmand (1800 km^2) occurred one month later (April 1991). The area

328 of Hamun-i Hirmand in March 1991 was 1700 km^2. The largest area for Gaud-i Zirreh in 1991 was
329 2600 km^2 observed four months later in July. Therefore, the time lags for water conveyance from
330 Hamun-i Puzak and Hamun-i Saburi to Hamun-i Hirmand and finally to Gaud-i Zirreh were almost
331 one and four months, respectively. Additionally, the maximum area of Gaud-i Zirreh was 3000 km^2,
332 which occurred more than 25 months later (in June 1993) because of accumulating inflows in the
333 preceding years.

334 ***3.4. Drought in the Hirmand River sub-basin***

335 The large gap between SPI and SDI occurs after 2004. The correlation coefficients before and
336 after this year are 0.70 and 0.13, respectively reveals a drastic change in the relationship between
337 upstream precipitation and downstream (in the border) inflow. This gap between precipitation and
338 inflow continues until the SPI-SDI correlation becomes negative (i.e., -0.63 after 2010). Before 1990,
339 SDI values were almost always (except 1962 and 1984) larger than SPI (on average 0.65 larger) (Figure
340 5-a). However, after 1990, the SDI was lower than SPI (except 1994, 1998, 1999 and 2005). The
341 average difference between SDI and SPI was -0.9, -1.6 and -2.2 after 1990, 2004 and 2010 respectively
342 (Figure 5-a). Based on Table 1, these gaps between the two indices will considerably affect the dry or
343 wet classification of the year. For example, in water year 2014-2015, SPI has the highest value
344 indicating an extremely wet year in terms of upstream precipitation. However, in this year and based
345 on inflow at the border, SDI is less than -1 which implies a moderately dry year.

346 The mean annual precipitation in the whole Hirmand sub-basin (Figure 1-a) has the highest
347 correlation with the precipitation upstream of Kajaki Dam (≈ 0.97, Figure S 4). The mean
348 precipitation in the Hindu Kush mountainous region is higher than other parts of the basin (Figure S
349 3-b); however, the correlation between precipitation in mountainous parts of the basin and lower
350 regions downstream of Kajaki Dam is low ($\approx 40\%$). In other words, according to SPI, the wet and dry

cycles in the Hirmand sub-basin are governed by precipitation amounts in the upper parts of the sub-basin rather than downstream of Kajaki Dam (Appendix B). This means that wet conditions maybe observed upstream of Kajaki Dam while downstream portions of Hirmand River may be characterized by dry condition based on precipitation. High climatic variation of the Helmand Basin is important because the runoff in the upstream wet snow climate (Ds) and warm temperate climate (Cs) is a major contributor to the area of Hamun Lakes in the lower desert climate (BW). Also, the monthly distribution of precipitation in the Helmand Basin shows that March is often the wettest month of the year (Figure 5-d) even though the highest inflow of the river at the border occurs more frequently with some time lag in April or May (more detail in Appendix C).

3.5. Investigation of the lakes area in similar years in terms of inflow

After a long drought period between 1998-2004 (Figure 5-a), the Hamun Lakes changed from permanent waterbody to seasonal (Figure 2-a to d). Therefore, the lakes area in similar years in terms of inflow before and after the drought period has changed significantly (Figure 6). Also, in year 2008, CNR4 is inaugurated. The capacity of this reservoir is more than 0.8 km3, i.e. 40% of annual Hirmand River flow into Iran in the last 10 years. This reservoir has increased the water regulation capacity in the region to more than double from 0.65 to 1.45 km3, which can affect the area of the Hamun Lakes. In this regard, we compared the state of the lakes' area in similar hydrological conditions in terms of Hirmand River deliveries to Iran before and after drought period, i.e., 1992/2016, 1996/2009 and 1993/2011 (Figure 6- to c).

In 1992 ($inflow \approx 4$ km^3), the area of Hamun-i Hirmand, Hamun-i Saburi and Hamun-i Puzak were 1600, 1500 and 1000 km^2, respectively, which decreased by 55, 43 and 87% in a similar condition in 2016 (Figure 6-a). In 2009 ($inflow \approx 2.5$ km^3) Hamun-i Hirmand lost 86% of its area compared to 1996 (Figure 6-b). The areal loss of this lake in 2011 ($inflow \approx 2$ km^3) was 95% compared to 1993

374 (Figure 6-c). Likewise, the area of Hamun-i Puzak and Hamun-i Saburi decreased 57 and 45% in 2011
375 compared to similar conditions in 1993 (Figure 6-c). However, the gap between area of Hamun-i
376 Saburi and Hamun-i Puzak in 1996 and 2009 decreases. In 2009, only 19 and 11% of these lake's
377 areas, respectively, were lost compared to 1996 (Figure 6-b). There are no streamflow data available
378 for other rivers that feed the Hamun Lakes but water presence in a wetland in the northeast of Hamun-
379 i Puzak (Figure 6-b) shows considerable inflow from Khash River and likely other rivers in the north
380 (Figure 1-b). Since 2009, more than 70% of this wetland was full (even more than its area in 1996).
381 However, the wetland was dry in all other years after CNR4 operation and 2009 is an exception.

382 ***3.6. Monthly response of Hamun Lakes area to Hirmand River flow***

383 Monthly inflow can largely affect the area of Hamun-i Puzak and Hamun-i Saburi in the same
384 month (Figure 7-a and b) because water retention time in connected Hamun Lakes above Shile Canal
385 is small due to their low depth (shown in Figure 3 and Figure 4). When monthly Hirmand flow at the
386 border is less than 0.5 km^3, the area of Hamun-i Puzak is most likely to be less than 500 km^2 (Figure
387 7-a). Also, when inflow increases from 0.5 to between 0.5-1 km^3, the area is more probable to exceed
388 500 km^2. Also, Hamun-i Saburi is expected to be larger than 500 km^2 when inflow in border rises from
389 below 0.5 to above 0.5 km^3 (Figure7-b). The area of this lake increases to more than 1250 km^2 when
390 the Hirmand River delivery to Iran exceeds 1 km^3. Likewise, areas greater than 500 km^2 are expected
391 for Hamun-i Hirmand when inflow increases (Figure 7-c). Boxplots of Hamun-i Hirmand and Gaud-i
392 Zirreh have a considerable overlap (Figure 7-c and d) so there is no specific relation between Hirmand
393 River inflow in border and their area in the same month. The areas of Hamun-i Hirmand and, especially
394 Gaud-i Zirreh were very low after 2000 (Figure 2-c and d), indicating that Hirmand River inflow does
395 not reach these lakes and such comparison is not possible. Gaud-i Zirreh has higher water retention

time which resulted in higher dependence of this lake's area to water accumulation in preceding months.

4. Discussion

Hamun Lakes are responding to a shift in water management paradigm in a hydro politically complex transboundary basin where competition over limited water resources is on the rise. The new paradigm is intensified after 2004 which has marginalized environmental flows to the lake as detected by large the gap between SDI and SPI. The lakes are experiencing exacerbated environmental flow stress mainly due to human modifications and flow regulation. The continuation of this trajectory is expected to amplify adverse environmental, socio-economic, and public health impacts associated with more frequent and prolonged desiccation of the lakes. It is urgent to recognize environmental water security as an important element of region's sustainability and plan practical steps to increase binational cooperation to prevent extensive socio-ecological impacts.

The high correlation between SPI and SDI from 1960-2003 shows that high precipitation naturally will lead to high runoff in the Hirmand River sub-basin. The large discrepancy between SPI and SDI after 2004 is a strong evidence about the effects of recent anthropogenic modifications on the Hamun Lakes. Water regulation upstream of the Hirmand River in Afghanistan has become more intensive, decreasing the deliveries to Iran as a new phenomenon in the basin. As an example, before 2010, the maximum recorded annual precipitation of the Hirmand River sub-basin was 330 mm in water year 1989-1990, which led to the maximum flow into Iran since 1960 (i.e., 12 km^3). While the annual precipitation water year 2014-2015 (473 mm) was 40% larger than the 1990 rainfall, the Hirmand River inflow in the border in this year was 30% of the flow delivered in 1990 (i.e., less than 4 km^3), indicating greater upstream regulation in Afghanistan. Reduction of the Hirmand River flow to Iran has been attributed by Afghanistan to a reduction in precipitation (Mianabadi et al., 2020). We showed

in this study that annual precipitation over the basin increased significantly after 2000 (Figure 5-a and Figure S 2). Likewise, using remote sensing data on historical for 34 years, Mianabadi et al. (2020) showed that the frequency and amount of heavy precipitation have been increasing over the mountainous areas which are the main source of the Hirmand River flow. Also, the total irrigated area in the Hirmand River sub-basin between the Kajaki Dam and the border has increased 62% from 1990 to 2011 (Hajihosseini et al., 2020), significantly increasing the upstream agricultural water demand.

Increased regulation of Hirmand River flow in this transboundary basin has weakened the hydrologic conditions to sustain the lakes. Based on the inflow of Hirmand to Iran, three major hydrological droughts occurred in the 1970s, 1980s and 2000s (Figure 1-e). These droughts prompted the Iranian government to sign a treaty with Afghanistan in 1973 to share Hirmand River flow, construct CNR1-3 in 1983, and CNR4 in 2008 to store water to meet regional demand, i.e., domestic and agricultural uses. The cumulative capacity of CNRs ($\approx$1.5 km^3) plus 0.3 km^3 of annual evaporation from their surfaces amounts to about 95% of the annual average inflow of Hirmand River to Iran from 1995-2016 ($\approx$1.9 km^3 shown in Figure 1-e). While CNRs have been effective in helping meet the water demand in the Sistan region, they have created a tradeoff by causing the area of the Hamun Lakes to decline. The large area of CNRs (Figure 2-e to h) in all years (except extremely dry years in 2000 and 2001), regardless of the SDI value, is an artifact of the priority given to filling the CNRs as much as possible to meet water demands in Iran. Once CNRs are full, the overflow is conveyed to Hamun Lakes. Low monthly areal variation of CNRs compared to Hamun Lakes denotes their importance for water supply, which is an impetus for more than doubling the capacity of the CNRs in 2008 by adding CNR4. Quantifying the explicit effect of CNR4 on the lakes is complicated by the lack of flow data from all the tributaries as previously mentioned in section 2.4. However, the surface areas of Hamun-i Puzak and Saburi are quite sensitive to monthly inflow variation of 0.5 km^3

(60% of CNR capacity). For example, average area of Hamun Puzak and Saburi can be doubled if monthly flow of the Hirmand River increases from below 0.5 to between 0.5-1 km^3 (Figure 7-a and b). This illustrates the environmental water stress caused by diverting up to 0.81 km^3 to be stored in CNR4. A recent study reported that, from 2010-2019, when all the anthropogenic pressures in the basin were in full effect, the average surface area of the Hamun Lakes could be 112% larger without water diversion by CNR4 (ModaresiRad et al., 2022).

The effects of increased water regulation propagate back into Afghanistan in the lower elevation downstream most sections of the basin. Gaud-i Zirreh, which is more resistant to desiccation than other lakes, nearly dried out after 2005 prior to the operation of CNR4. For example, although, inflow in 1993 is less than 1992, Gaud-i Zirreh area is highest in 1993 ($\approx$3000 km^2) because accumulated water from extremely wet (1990: $inflow \approx 12$ km^3) and mildly wet (1991: $inflow \approx 5$ km^3 and 1992: $inflow \approx 4$ km^3) years. Therefore, the desiccation of Gaud-i Zirreh should mainly be attributed to Hirmand River regulation in Afghanistan (annual inflow decreased from 4 to 1.9 km^3 shown in Figure 1-e) which is worsened by reservoir construction in Iran (CNR4) and Afghanistan (Kamal-Khan dam) next to border.

In the last two decades, the agricultural water consumption in the studied area has increased over three times. Share of Afghanistan is about 90 percent of the total consumed water in agriculture sector. As a rule of thumb, in the Helmand Basin, irrigating 1000 km^2 cropland consumes 1.1 km^3 water (Akbari and Haghighi, 2022). More than 1700 km^2 of cropland development is planned to be irrigated by the Kamal-Khan Dam in the future (Mianabadi et al., 2021) which requires about 2 km^3 water. Therefore, the agricultural water needs will further increase on the Afghanistan size over time. Eight reservoirs in the basin (Figure 1-a) with a collective water storage capacity of more than 4.5 km^3 (share of Afghanistan 67%) regulate flow intensively. The lakes are desiccating despite the fact that the

Hirmand River inflow at the international border has averaged 1.9 km^3 (1995-2016), twice the designated flow in the 1973 treaty. This indicates that the designated amount of water delivery in the treaty from Afghanistan and frequency and timing of deliveries do not suffice to meet both human water demands on the Iranian side while providing environmental flows to the lakes. The inauguration of Kamal-Khan dam in March 2021 adds another knob to control the magnitude and timing of flow deliveries to Iran, which could increase downstream stress and aggravate the condition of the lakes. It is time to clarify the environmental dimensions of the 1973 treaty in light of changing water supply and demand conditions on both sides of the border.

The 1998-2004 drought was the most severe on record going back to 1830 (Williams-Sether, 2008). After this dry period, the frequency and severity of dust storms has significantly increased (Rashki et al., 2012). This affects the livelihood of more than 1.1 million people who rely on Hirmand River inflow and Hamun Lakes in the Sistan region (Rashki et al., 2013). More than 25% of the population migrated from Sistan region due to environmental and economic situation after Hamun Lakes desiccation (ICANA, 2015). In 1977 more than 55% of Sistan inhabitants in Iran worked in the agricultural sector but this ratio has reduced to less than 22% in 2015 due to water scarcity and droughts (Ministry of Cooperatives Labour and Social Welfare Iran, 2017). Drought has negatively impacted fisheries which have been brought to a halt (Rashki et al., 2012) and caused high unemployment (ICANA, 2012). The unemployment and declining quality of life can undermine border security due to potential links to unlawful economic activities, and in some cases terrorism (Bagchi and Paul, 2018). The desiccation of the Hamun Lakes has hydro political, ecological, climatic, socio-economic, and legal complexities that go far beyond a hydrological assessment. Nonetheless, the results of this investigation shed light on the hydroclimatic aspects of this vulnerable socio-ecological system, calling for action and further interdisciplinary research to understand the root causes and potential consequences of the desiccation of the Hamun Lakes to inform mitigation efforts.

5. Conclusions

Hamun Lakes are connected water bodies consisting of three connected Lakes (Hamun-i Puzak, Hamun-i Saburi and Hamun-i Hirmand) above Shile Canal and a deeper terminal lake (Gaud-i Zirreh). The first three cascading lakes are very shallow, and they respond rapidly to monthly Hirmand River inflow variation. A shift in upstream regulations of the Hirmand River in Afghanistan has changed post-2004 water deliveries at the international border. From 1960 to 2003, Standardized Discharge Index (SDI) and Standardized Precipitation Index (SPI) were highly correlated (70%), meaning high river flow was expected to feed the lakes due to high precipitation over the Hirmand River sub-basin. However, the correlation changed to 0.13 in the periods 2004-2016 indicating a drastic decline in the Hirmand River flow downstream despite large amounts of upstream precipitation over its sub-basin. This gap kept increasing and SPI-SDI correlation became negative (≈ -0.63) between 2010-2016. Upstream regulations are the main cause of inflow delivery reduction to the lakes. The construction of Chah Nimeh Reservoir 4 (capacity of 0.81 km^3 for domestic and agricultural use in a socio-economically disadvantaged region of Iran) and Kamal-Khan Dam (capacity 0.05 km^3) has aggravated the situation. The decline of the socio-ecological system due to unsustainable water management in this transboundary region is expected to have detrimental impacts on the condition of the residents (e.g., dust storms). Therefore, revisiting the 1973 treaty between riparian countries to share the Hirmand River inflow considering the environmental right of the lakes is recommended to improve the condition of the region.

Acknowledgement

The authors are thankful to Dr. Kaveh Madani for his valuable comments. The second author acknowledges the Iranian and Persian Gulf Studies professorship from Oklahoma State University's School of Global Studies and Partnerships.

Funding

This work was supported by the University of Oulu Graduate School (UniOGS).

Supplementary materials

All Google Earth Engine Java Script API source codes are available below:

- For extracting DEM and Urban:
https://code.earthengine.google.com/fd8607d4c9d79f1ae6ae6d712877c877?noload=true
- For monthly and annually water body detection from 1987 to present:
https://code.earthengine.google.com/76d2a59d4b05979fc583bd16573fc65e?noload=true
- For precipitation calculation:
https://code.earthengine.google.com/5e14fcbbff9e0828b698340f58eb9628?noload=true

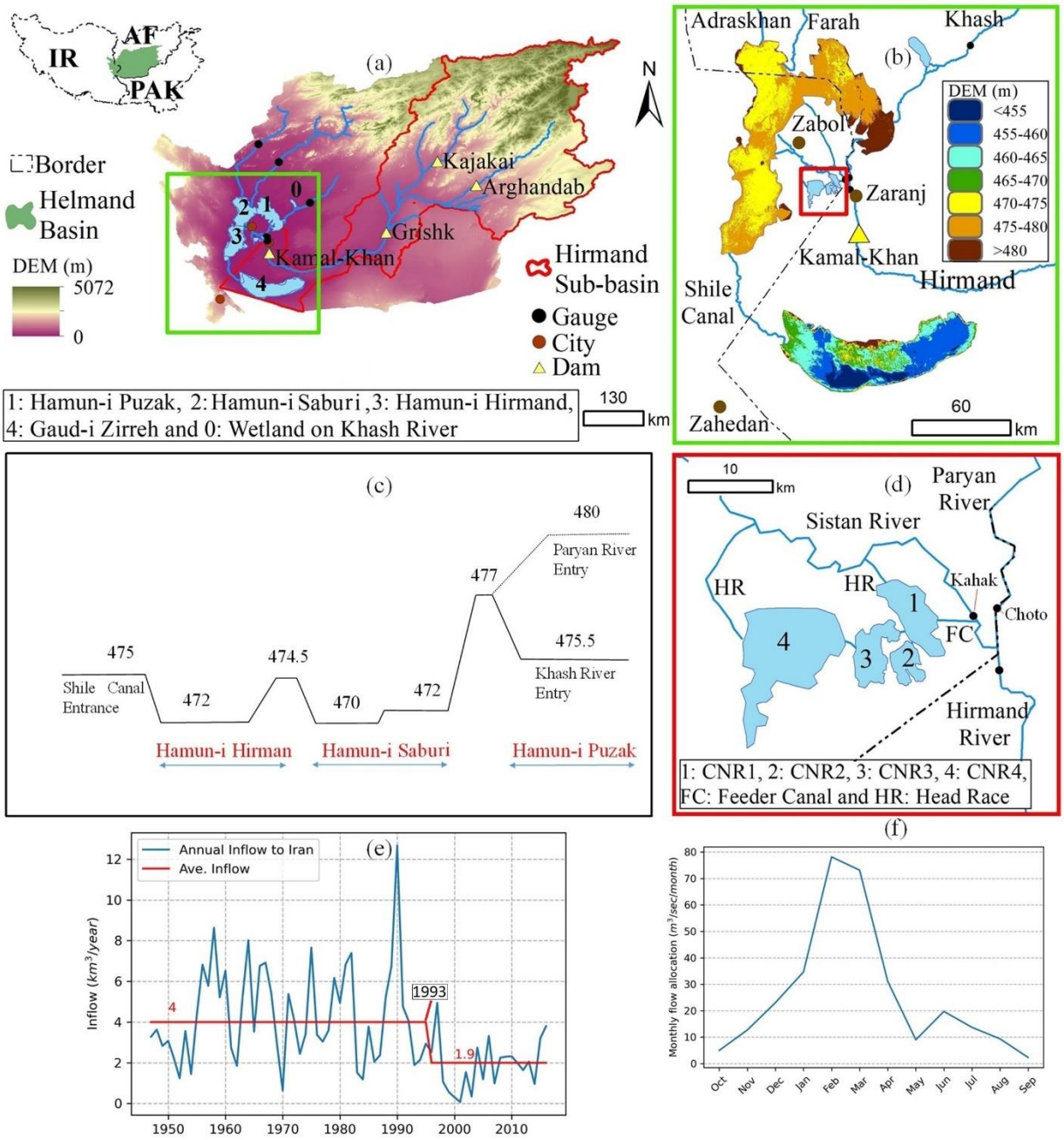

Figure 1. Study area: a) Helmand Basin, Hirmand River sub-basin and Hamun Lakes with the location of dams, inflow gauges and cities, b) DEM of Hamun Lakes and close water bodies to Hamun Lakes, c) transverse profile of Hamun Lakes HIWRI, 2017), d) Hirmand, Sistan and Paryan Rivers next to border between Iran and Afghanistan, CNRs, Head Races and Feeder Canal, e) annual inflow of Hirmand River in the location of Iran-Afghanistan border from 1960 to 2016 (average flow shift in 1993) and f) guarantied monthly Hirmand River flow to reach Iran based on the bilateral treaty between Iran and Afghanistan in 1973 (ref: MoE, 2013)

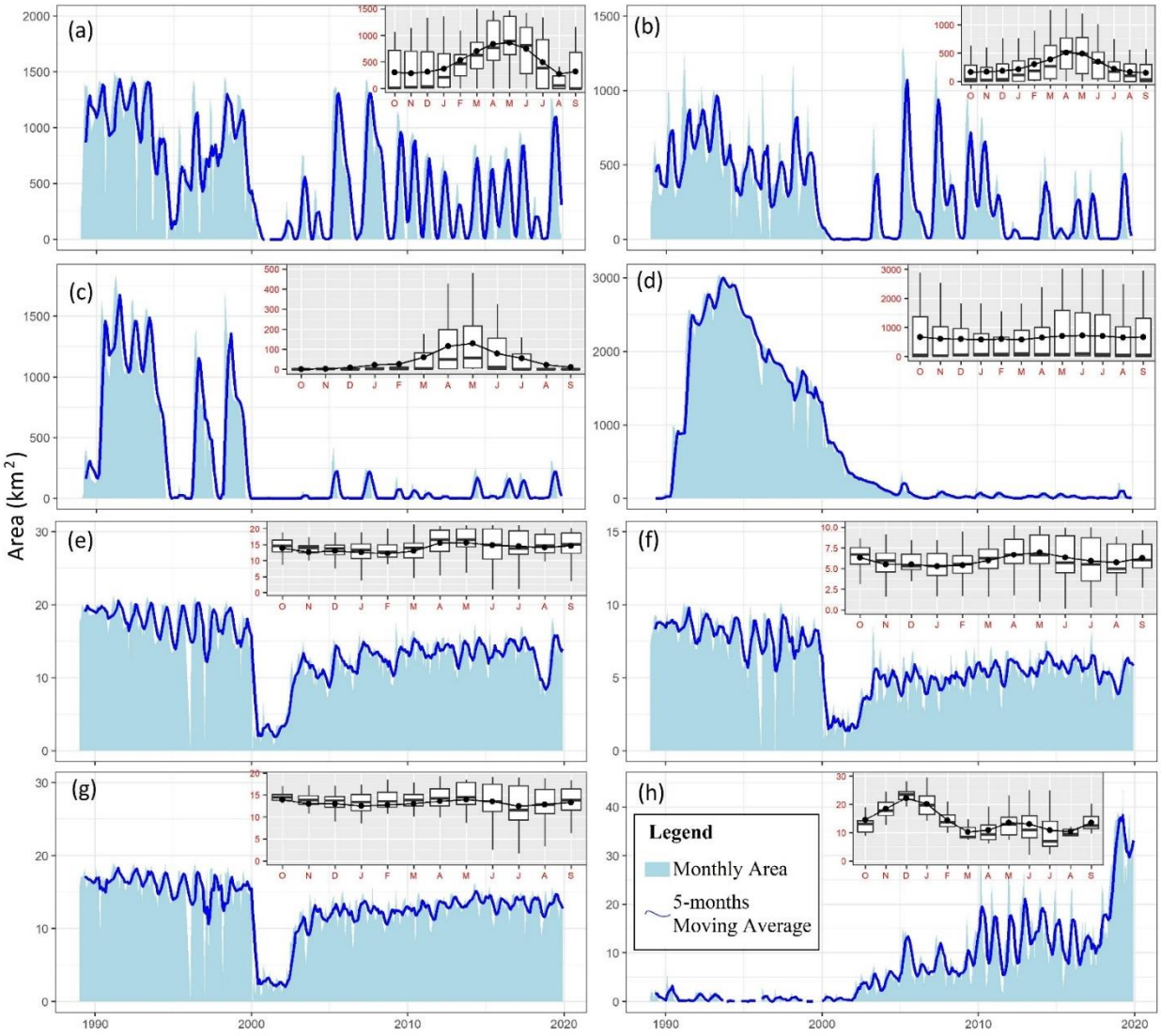

Figure 2. Monthly area with box plot of area in each month for: a) Hamun-i Saburi, b) Hamun-i Puzak, c) Hamun-i Hirmand, d) Gaud-i Zirreh, e) CNR1, f) CNR2, g) CNR3 and h) CNR4

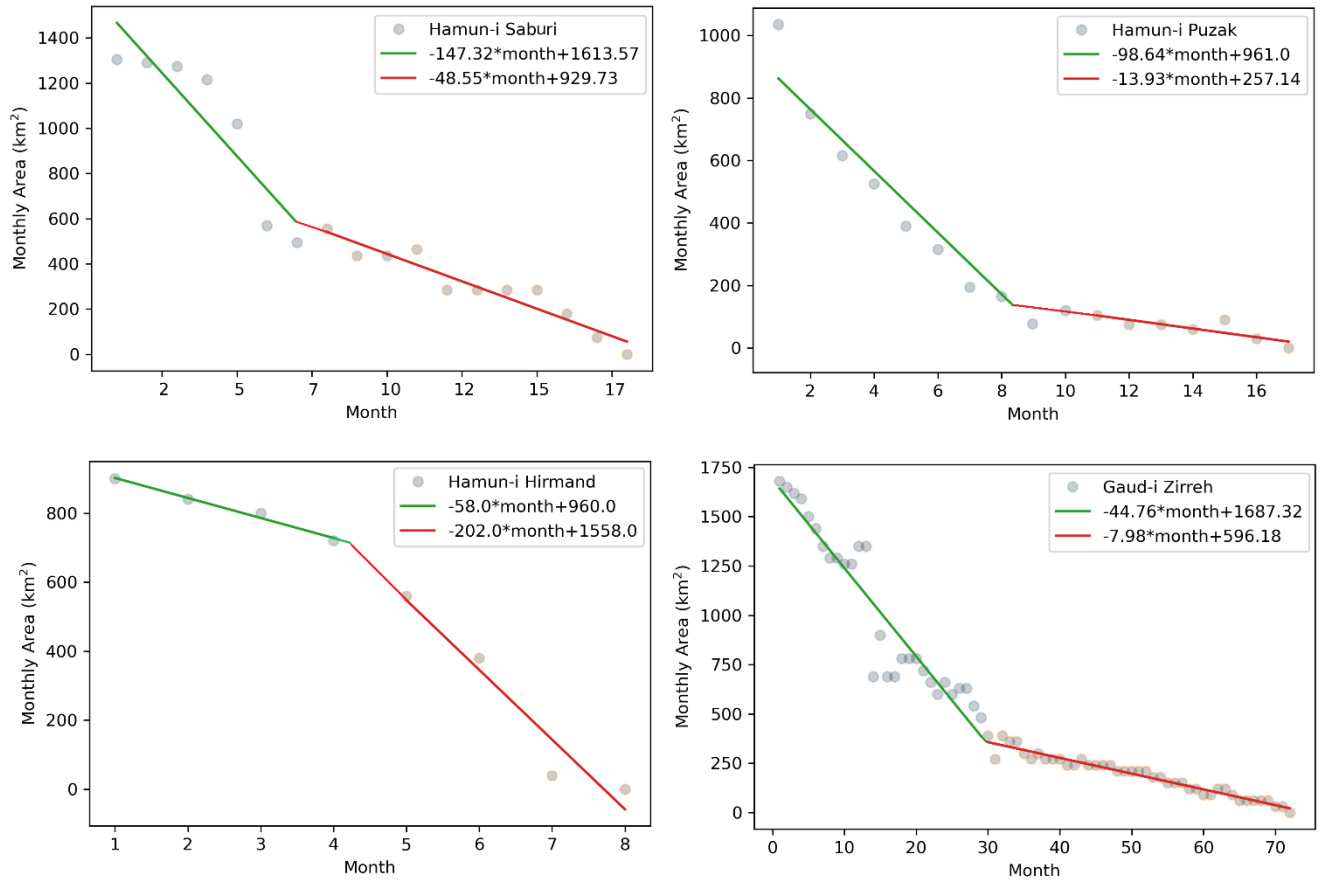

Figure 3. Desiccation of Hamun Lakes rate based on number of months passing from March 1999 when inflow became zero to each of lake

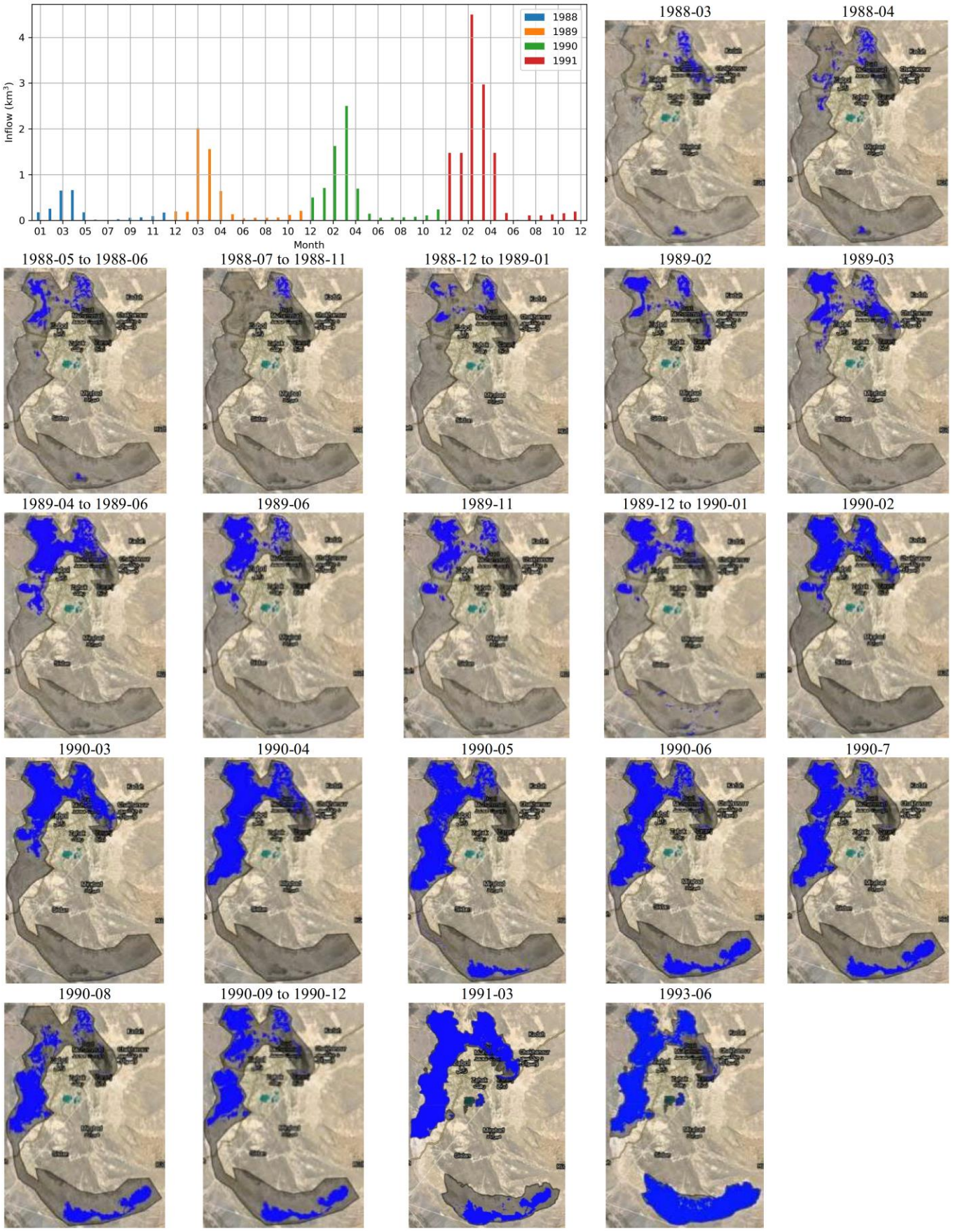

Figure 4. Water transfer between Hamun lakes (images are produced by Google Earth Engine Java Script API)

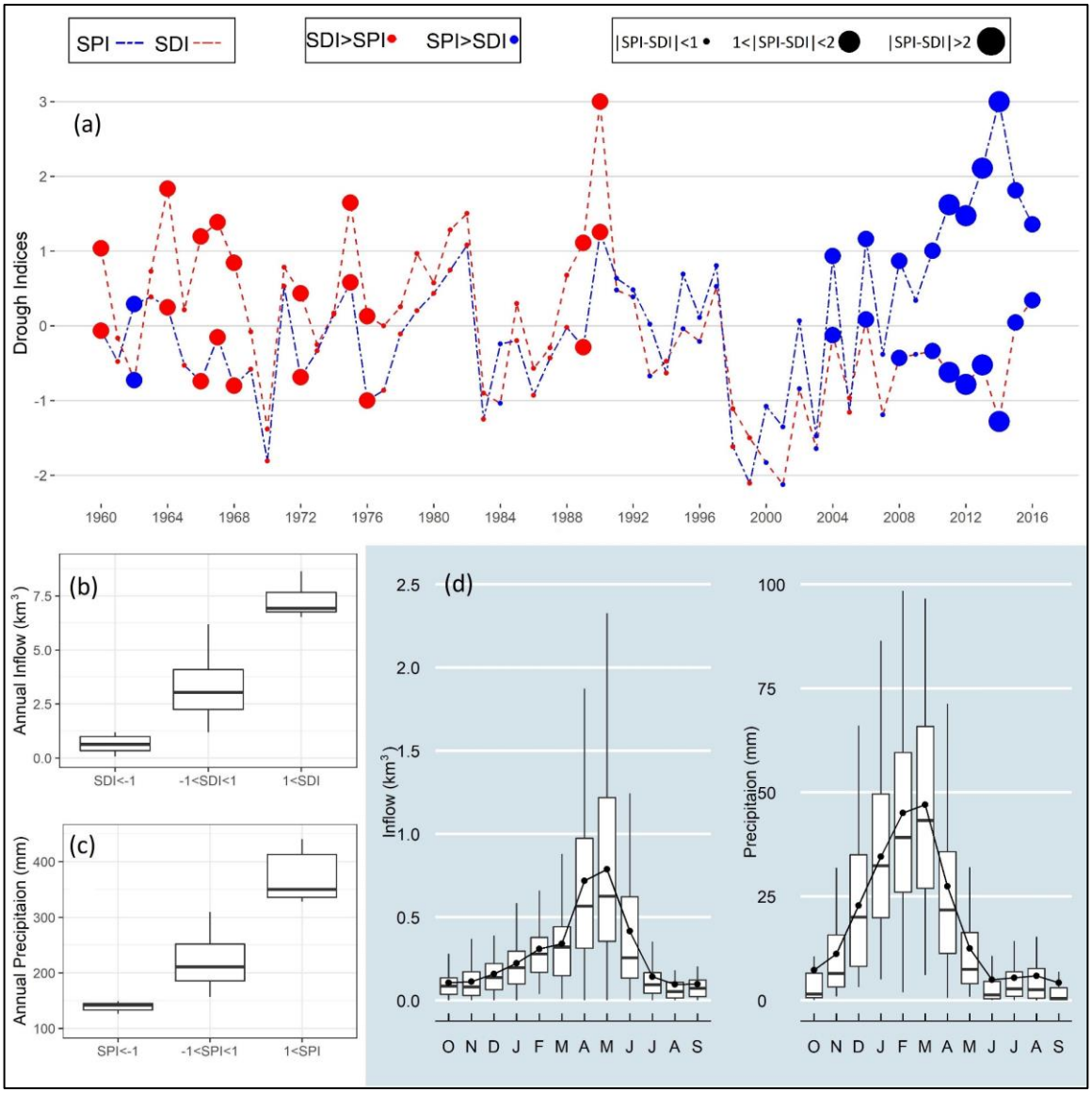

Figure 5. a) SPI and SDI of Hirmand River sub-basin from 1960 to 2016 with difference of SPI and SDI in each year showing a shift in water management paradigm after 2003 when high precipitation does not correspond to high Hirmand River inflow in the location of border, b) annual precipitation based on different intervals of SPI c) annual inflow based on different intervals of SDI and d) the long-term monthly boxplots of Inflow and precipitation

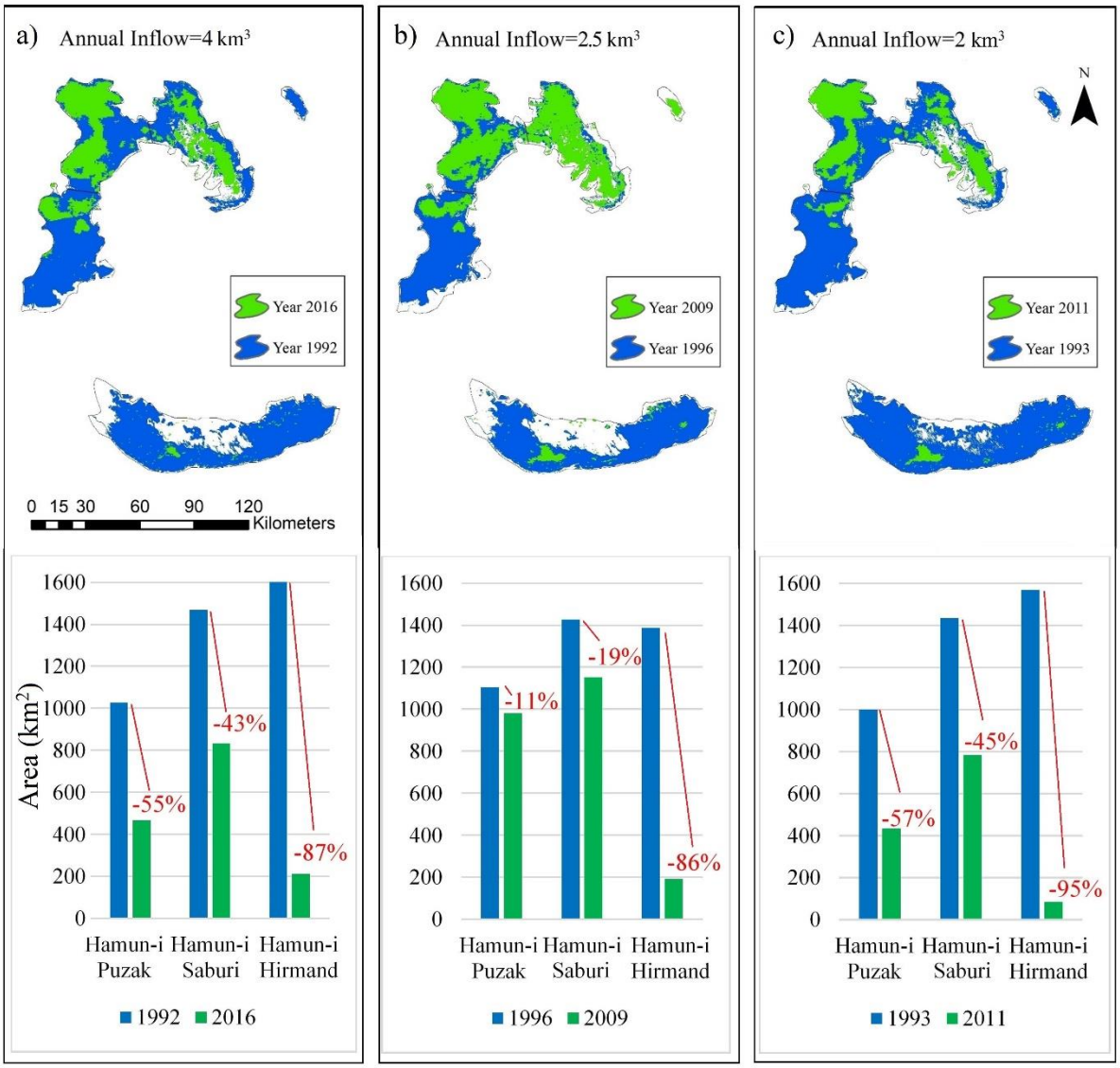

Figure 6. Comparison between areas of the Hamun Lakes in similar years in terms of the Hirmand River annual inflow delivery in the border; percentage of area decline before and after long dry period (1998-2004) are shown in each bar plot

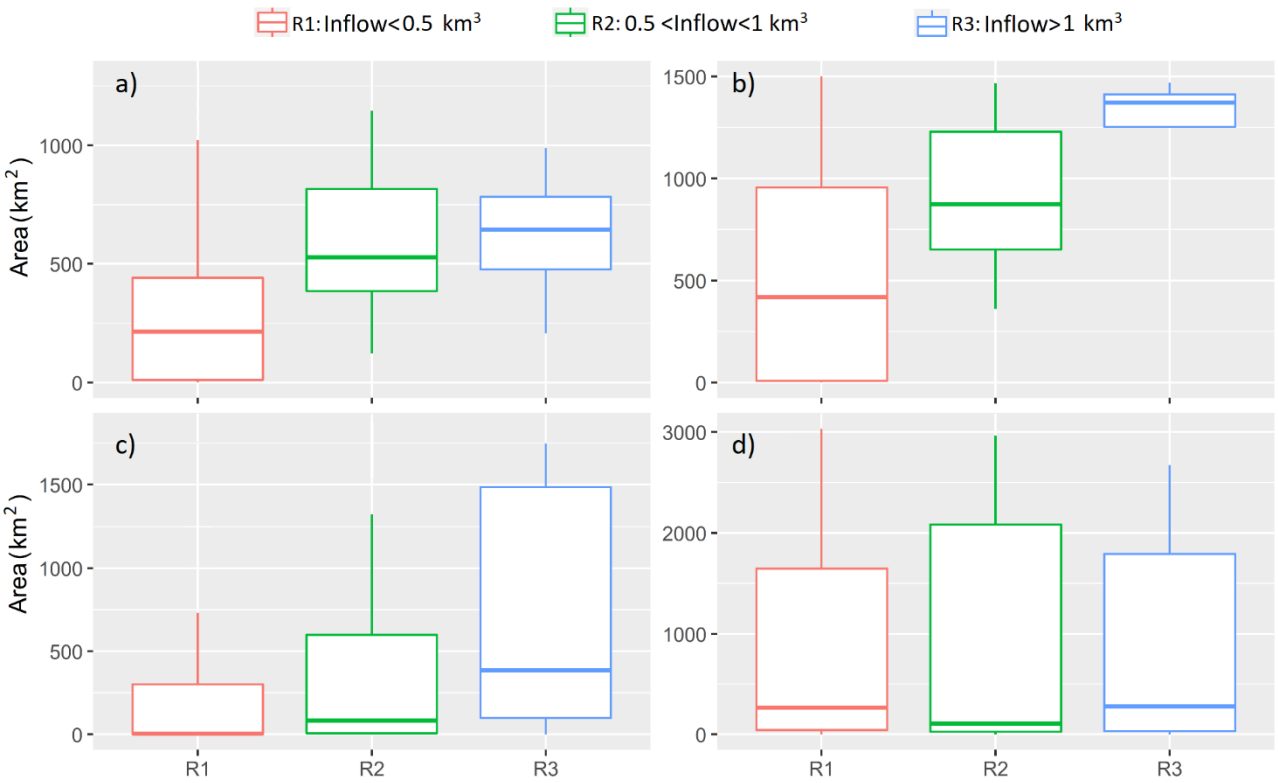

552
553 Figure 7. Consequence of incrementally increasing Hirmand River monthly inflow by 0.5 km^3 on
554 area of a) Hamun-i Puzak, b) Hamun-i Saburi, c) Hamun-i Hirmand, and d) Gaud-i Zirreh

555

556 Table 1. Different categories of climatological conditions based on the SPI and SDI values

Category	*Range of drought indices (SPI/SDI)*
Extremely wet	More than 2.00*
Very wet	1.50–1.99*
Moderately wet	1.00–1.49*
Mildly wet	0.00–0.99*
Mild drought	–0.99 to 0.00*, **
Moderate drought	–1.49 to −1.00*, **
Severe drought	–2.00 to −1.50*. **
Extreme drought	<–2.00*, **

**Lloyd-Hughes and Saunders (2002). **McKee et al. (1993).*

557

Appendix A. Inflow of main rivers of Helmand Basin

Köppen-Geiger climate classification map in Helamad Basin and location of main rivers and their last gauges area shown in Figure S 1-a. Inflow of main rivers of Helmand Basin in Afghanistan observed in last gauges of each of them from 1954-1979 are also shown in Figure S1-b based on USGS (Williams-Sether, 2008). Based on this figure, the Hirmand River provides 70 percent of the total flow to the lakes and the rest is from the Farah River[†]. However, Iran Department of Environment (DOE, 2014) reported that the share of the Hirmand River is about 90 percent. Estimating the exact share of Hirmand River is challenging due to lack of data and transparency in the basin.

[†] The Pearson correlation coefficient for annual inflow between Farah and Hirmand Rivers during 1955-1980 is 0.82

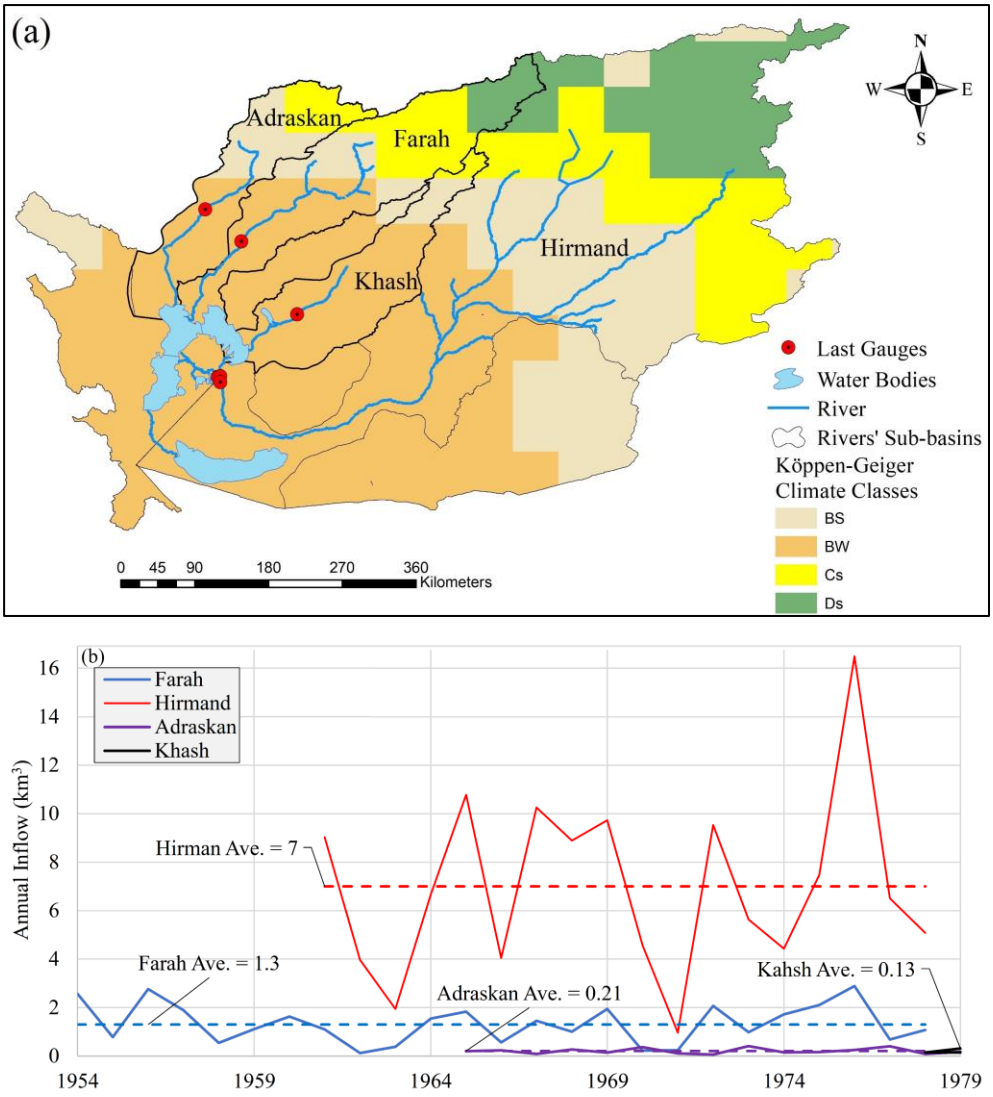

Figure S 1. a) Main rivers of Helamad Basin, their sub-basins with the location of last gauges on each of them and Köppen-Geiger climate classification map, b) Inflow of main rivers of Helmand Basin in Afghanistan observed in last gauges of each of them (retrieved from https://afghanistan.cr.usgs.gov/water)

Appendix B. Precipitation and potential evapotranspiration over Hirmand River sub-basin

We used SPI to capture trend of precipitation change. This index is based on the trend variation in precipitation. High correlation between well-known precipitation products, i.e., GPCC and PERSIANN-CDR (≈0.84) as well as GPCC and TRMM-3B43 (≈0.94), shows that changing data source of precipitation from GPCC to other products (e.g., PERSIANN-CDR) does not affect our SPI results considerably.

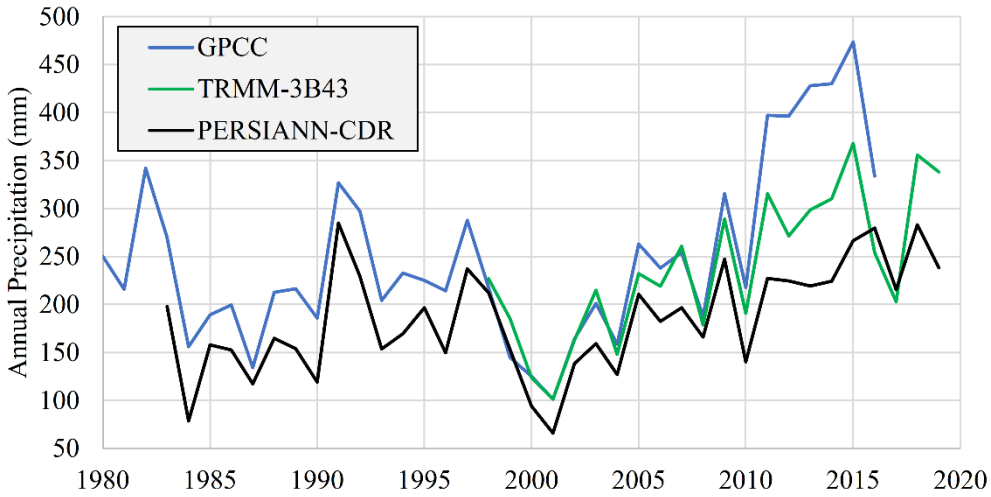

Figure S 2. Annual precipitation over Hirmand River sub-basin by different precipitation products

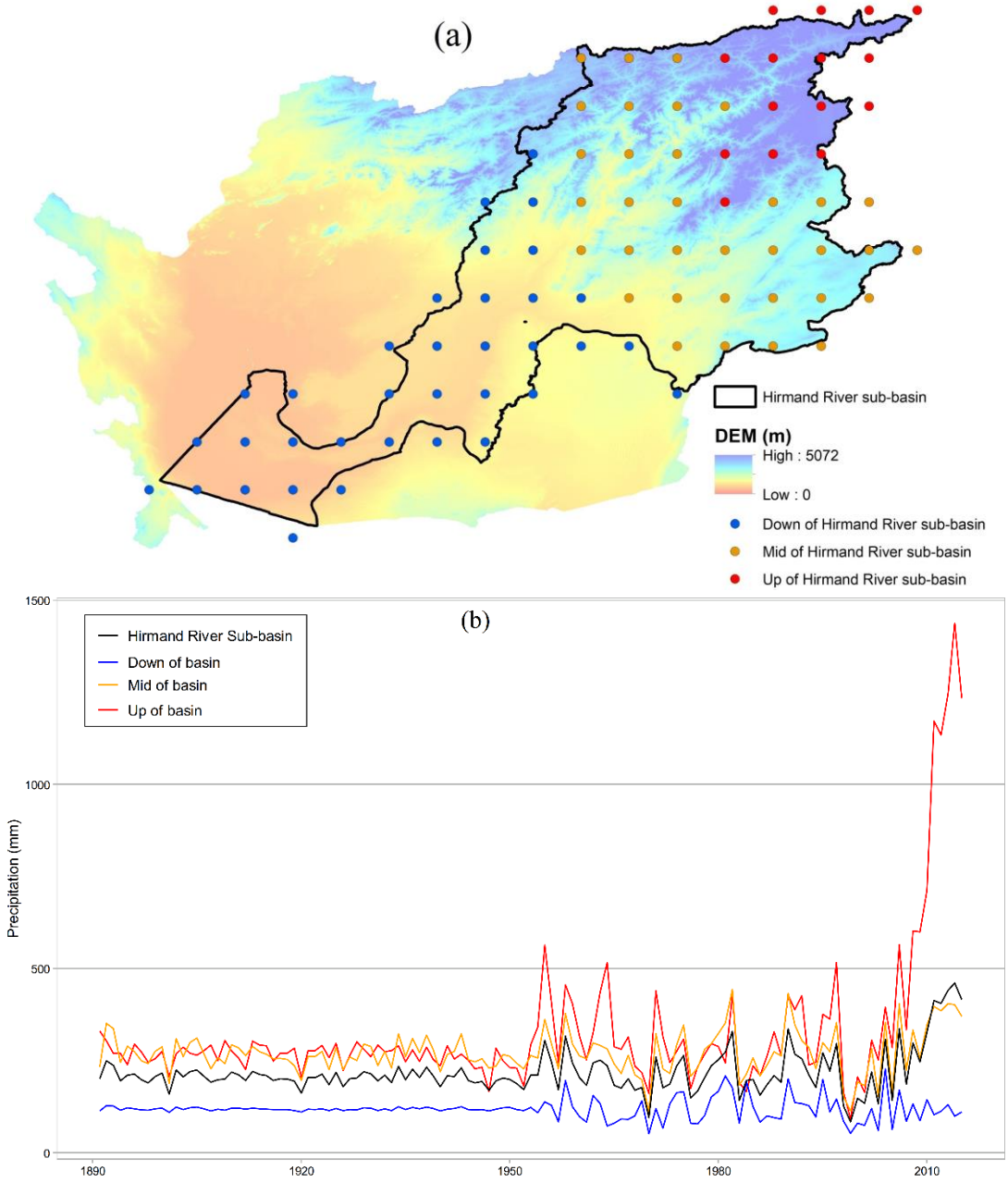

Figure S 3. a) Hirmand River sub-basin and DEM of Helmand Basin used to divide it to three regions: Up, Mid and Down based on elevation of regions, b) precipitation in all Hirmand River sub-basin, up, mid, and down regions calculated by GPCC

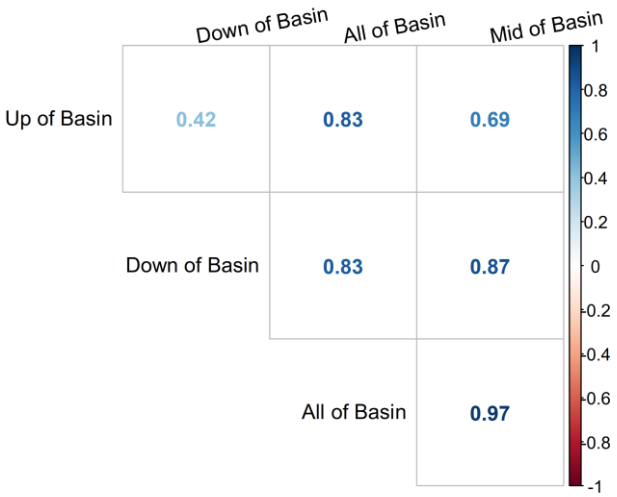

587
588 Figure S 4. Correlation of annual precipitation in different regions of Hirmand River sub-basin

589

Appendix C. Monthly inflow and precipitation

Precipitation is over Hirmand River sub-basin calculated by GPCC and inflow is measured in first gauge on Hirmand River in Iran next to border of Iran – Afghanistan. Based on below plots, 3rd quantile of precipitation in years with $SPI > 1$ is higher in Oct., to Jan.

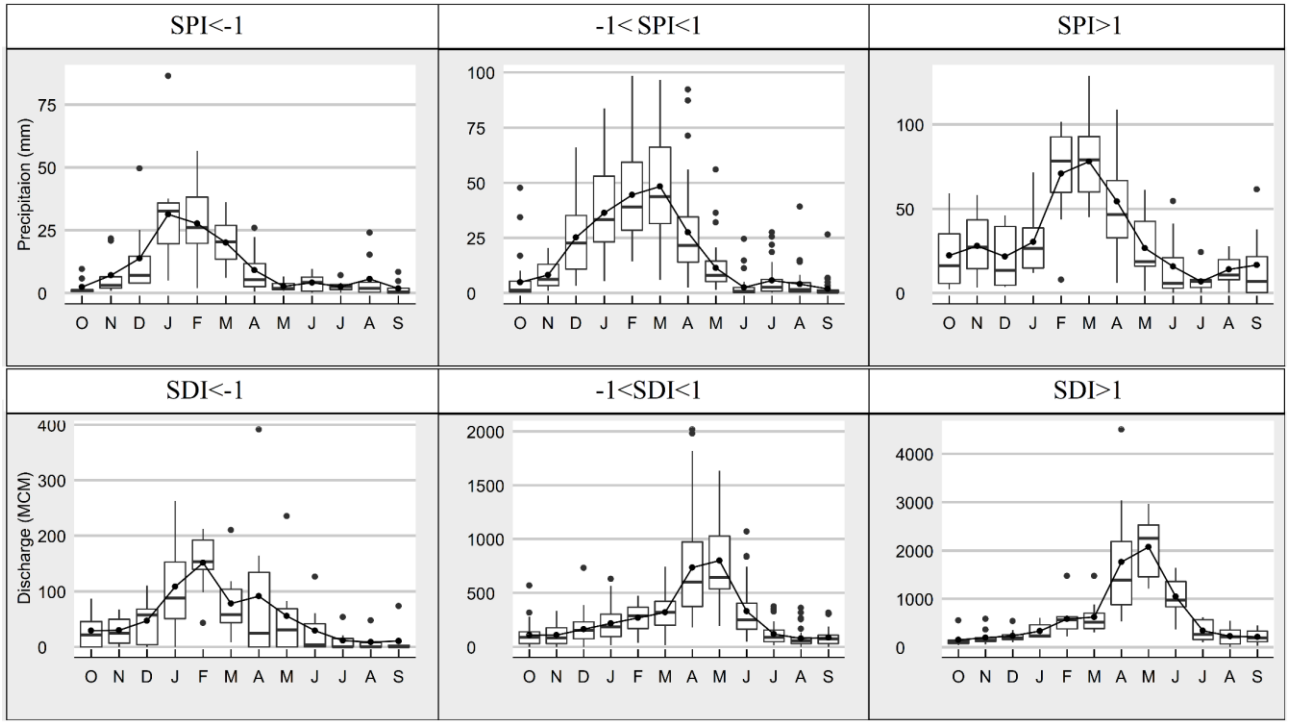

Figure S 5. Monthly distribution of precipitation and inflow in different years in terms of SDI/ SPI change

Appendix D. Comparison between SPI and SPEI

In calculation of SPI, evaporating effect is missing. Therefore, Standardized Precipitation Evapotranspiration Index (SPEI) is introduced which utilizes the difference between precipitation and Potential-Evapotranspiration (PET) in equation 3. We utilized PET from MOD16 dataset (https://lpdaac.usgs.gov/data/data-citation-and-policies/).

SPEI is mainly a measure of meteorological drought and may lead to biases in describing other categories of droughts (Sheffield et al., 2012). The comparison between SPI and SPEI, shown in below figure, approves that the result of them in terms of drought categorization is consistent because of zero bias and high correlation.

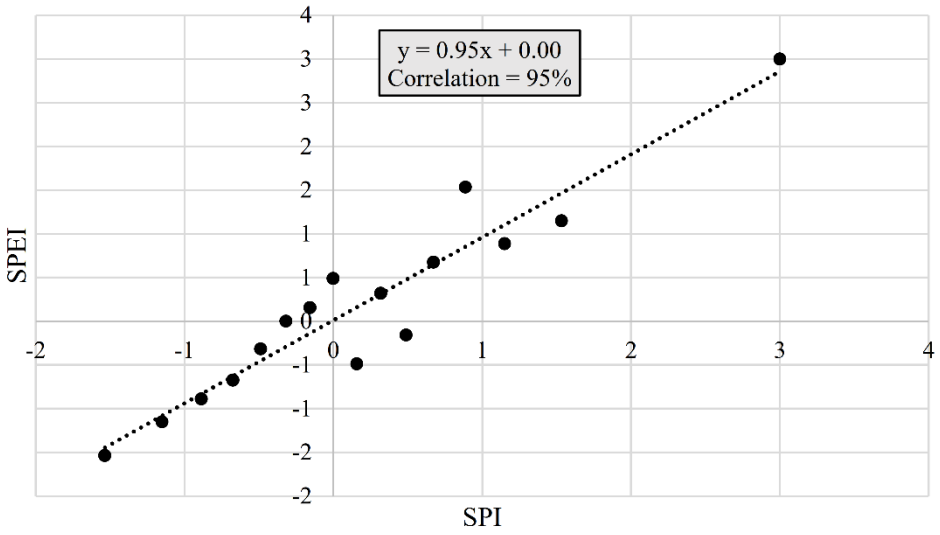

Figure S 6. Comparison between SPI and SPEI over the Hirmand River sub-basin

The Mann-Kendall Trend Test (null hypothesis: non-existing trend in the time series) using (*Kendall* R package) approved that there is no trend in PET ($p - value = 0.26$).

Appendix E. Best threshold for water detection by Normalized Difference Spectral Indices

Hamun Lakes are not gauged so there is no data on water level for them. Here we compared detected water body area using Normalized Difference Spectral Indices (NDSI) (i.e., NDWI and NDVI) and JRC Global Surface Water Mapping (Pekel et al., 2016) (https://global-surface-water.appspot.com/) using Google Earth Engine API. The JRC dataset is available for 1985-2019. Therefore, first we detected water body for the Hamun Lakes by different thresholds for NDWI and NDVI and then compared them with JRC. We used below accuracy metrics to determined best thresholds. A^{NDSI} and A^{JRC} are the estimated area by NDWI/NDVI and JRC respectively:

$$Corr. = \frac{cov(A^{NDSI}, A^{JRC})}{\sigma(A^{NDSI})\sigma(A^{JRC})} \quad (2)$$

$$RMSE = \sqrt{\frac{\sum_{t=1}^{T}(A_t^{JRC} - A_t^{NDSI})^2}{T}} \quad (3)$$

$$Bias = \frac{\sum_{t=1}^{T} A_t^{NDSI} - \sum_{t=1}^{T} A_t^{JRC}}{\sum_{t=1}^{T} A_t^{JRC}} \quad (4)$$

Result of this comparison verified that best threshold for NDVI and NDWI for water detection are NDVI<0.04 and NDWI>0.17 as shown in Figure S7-b. Different threshold than suggested one can result in overestimation (Figure S7-c) or underestimation (Figure S7-a) of area.

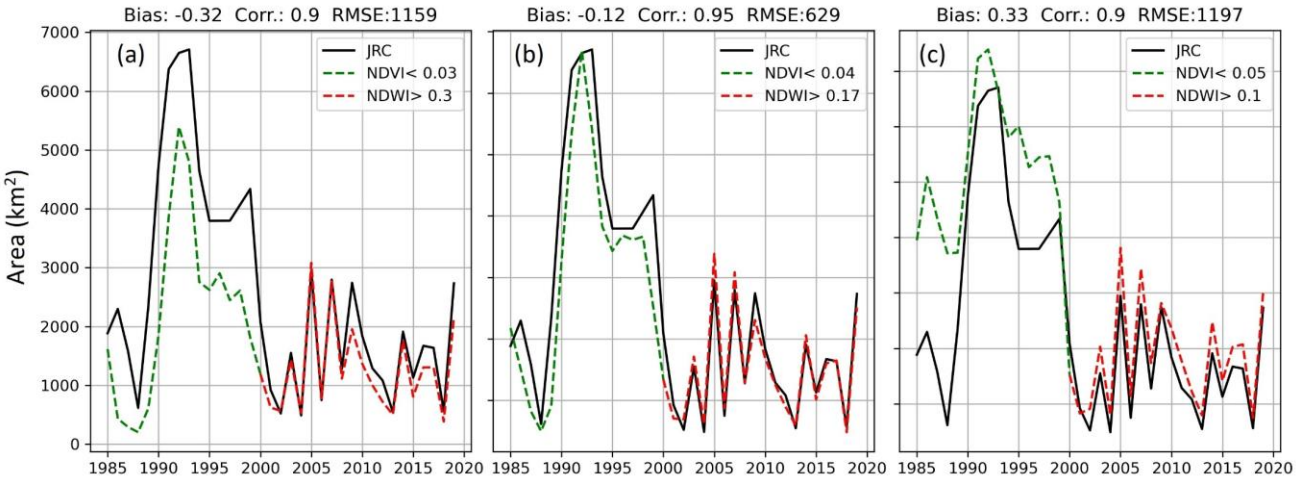

Figure S 7. Comparison between detected area by different thresholds for NDWI/NDVI and JRC

627 **References**

628 Absaran Consulting Company, 2015. Chah Nimeha water resources planning report, studies of the
629 second phase of water supply in Sistan plain.

630 Afganistan Ministry of Urban Development Affairs, 2015. The State of Afghan Cities Report 2015.

631 AghaKouchak, A., Norouzi, H., Madani, K., Mirchi, A., Azarderakhsh, M., Nazemi, A., Nasrollahi, N.,
632 Farahmand, A., Mehran, A., Hasanzadeh, E., 2015. Aral Sea syndrome desiccates Lake Urmia:
633 call for action. J. Great Lakes Res. 41, 307–311.

634 Ahlers, R., Brandimarte, L., Kleemans, I., Sadat, S.H., 2014. Ambitious development on fragile
635 foundations: Criticalities of current large dam construction in Afghanistan. Geoforum 54, 49–
636 58. https://doi.org/10.1016/j.geoforum.2014.03.004

637 Akbari, M., Baubekova, A., Roozbahani, A., Gafurov, A., Shiklomanov, A., Rasouli, K., Ivkina, N.,
638 Kløve, B., Haghighi, A.T., 2020. Vulnerability of the Caspian Sea shoreline to changes in
639 hydrology and climate. Environ. Res. Lett.

640 Akbari, M., Haghighi, A.T., 2022. Satellite-based Agricultural Water Consumption Assessment in the
641 Ungauged and Transboundary Helmand Basin between Iran and Afghanistan (under review).
642 Remote. Sens. Lett.

643 Akbari, M., Torabi Haghighi, A., Aghayi, M.M., Javadian, M., Tajrishy, M., Kløve, B., 2019.
644 Assimilation of satellite-based data for hydrological mapping of precipitation and direct runoff
645 coefficient for the Lake Urmia Basin in Iran. Water 11, 1624.

646 Alam, K., Trautmann, T., Blaschke, T., 2011. Aerosol optical properties and radiative forcing over
647 mega-city Karachi. Atmos. Res. 101, 773–782.

Alborzi, A., Mirchi, A., Moftakhari, H., Mallakpour, I., Alian, S., Nazemi, A., Hassanzadeh, E., Mazdiyasni, O., Ashraf, S., Madani, K., others, 2018. Climate-informed environmental inflows to revive a drying lake facing meteorological and anthropogenic droughts. Environ. Res. Lett. 13, 84010.

Amini, A., Ghoreishi, S.Z., Mianabadi, H., 2021. Understanding 1973 the Helmand Treaty by Invoking Rules of Interpretation According to Vienna Convention 1969. Dep. Water Irrig. Available online https//jwim. ut. ac. ir/article_82737. html (accessed 23 August 2021).

Ashouri, H., Hsu, K.-L., Sorooshian, S., Braithwaite, D.K., Knapp, K.R., Cecil, L.D., Nelson, B.R., Prat, O.P., 2015. PERSIANN-CDR: Daily Precipitation Climate Data Record from Multisatellite Observations for Hydrological and Climate Studies. Bull. Am. Meteorol. Soc. 96, 69–83. https://doi.org/10.1175/BAMS-D-13-00068.1

Bagchi, A., Paul, J.A., 2018. Youth unemployment and terrorism in the MENAP (Middle East, North Africa, Afghanistan, and Pakistan) region. Socioecon. Plann. Sci. 64, 9–20. https://doi.org/10.1016/j.seps.2017.12.003

Boschetti, M., Nutini, F., Manfron, G., Brivio, P.A., Nelson, A., 2014. Comparative analysis of normalised difference spectral indices derived from MODIS for detecting surface water in flooded rice cropping systems. PLoS One 9, e88741.

Chaudhari, S., Felfelani, F., Shin, S., Pokhrel, Y., 2018. Climate and anthropogenic contributions to the desiccation of the second largest saline lake in the twentieth century. J. Hydrol. 560, 342–353. https://doi.org/10.1016/j.jhydrol.2018.03.034

Chen, J.L., Wilson, C.R., Tapley, B.D., Save, H., Cretaux, J.F., 2017. Long-term and seasonal Caspian

669 Sea level change from satellite gravity and altimeter measurements. J. Geophys. Res. Solid
670 Earth 122, 2274–2290. https://doi.org/10.1002/2016JB013595

671 Chipman, J.W., Lillesand, T.M., 2007. Satellite-based assessment of the dynamics of new lakes in
672 southern Egypt. Int. J. Remote Sens. 28, 4365–4379.
673 https://doi.org/10.1080/01431160701241787

674 Dehgan, A., Palmer-Moloney, L.J., Mirzaee, M., 2014. Water security and scarcity: Potential
675 destabilization in western Afghanistan and Iranian Sistan and Baluchestan due to
676 transboundary water conflicts. Water and post-conflict peacebuilding 305.

677 Ehsani, M.R., Arevalo, J., Risanto, C.B., Javadian, M., Devine, C.J., Arabzadeh, A., Venegas-quiñones,
678 H.L., Paige, A., Oro, D., Behrangi, A., 2020. Hydroclimatological and Vegetation Variabilities 1–
679 18.

680 Farahmand, A., AghaKouchak, A., 2015. A generalized framework for deriving nonparametric
681 standardized drought indicators. Adv. Water Resour. 76, 140–145.

682 Ghajarnia, N., Akbari, M., Saemian, P., Ehsani, M.R., Hosseini-Moghari, S.-M., Azizian, A., Kalantari,
683 Z., Behrangi, A., Tourian, M.J., Klöve, B., others, 2021. Evaluating the Evolution of ECMWF
684 Precipitation Products Using Observational Data for Iran: From ERA40 to ERA5.

685 Gorelick, N., Hancher, M., Dixon, M., Ilyushchenko, S., Thau, D., Moore, R., 2017. Google Earth
686 Engine: Planetary-scale geospatial analysis for everyone. Remote Sens. Environ.

687 Goudie, A.S., Middleton, N.J., 2006. Desert dust in the global system. Springer Science & Business
688 Media.

689 Goudie, A.S., Middleton, N.J., 2000. Dust storms in south west Asia. Acta Univ. Carolinae, Suppl.
690 7383.

691 Haghighi, A.T., Kløve, B., 2015. A sensitivity analysis of lake water level response to changes in
692 climate and river regimes. Limnologica 51, 118–130.

693 Haghighi, A.T., Zaki, N.A., Rossi, P.M., Noori, R., Hekmatzadeh, A.A., Saremi, H., Kløve, B., 2020.
694 Unsustainability syndrome-from meteorological to agricultural drought in arid and semi-arid
695 regions. Water (Switzerland) 12. https://doi.org/10.3390/w12030838

696 Hajihosseini, M., Hajihosseini, H., Morid, S., Delavar, M., Booij, M.J., 2020. Impacts of land use
697 changes and climate variability on transboundary Hirmand River using SWAT. J. Water Clim.
698 Chang. 11, 1695–1711.

699 Hamoon International Wetland Research Institute of Zabol University (HIWRI), 2017. Investigation
700 of water requirement for Hamoon International Wetland in different water scenarios.

701 Hao, Z., AghaKouchak, A., Nakhjiri, N., Farahmand, A., 2014. Global integrated drought monitoring
702 and prediction system. Sci. data 1, 1–10.

703 Helmand Commission, 1973. The 1973 Helmand River Treaty [WWW Document]. URL
704 https://www.internationalwaterlaw.org/documents/regionaldocs/1973_Helmand_River_Wate
705 r_Treaty-Afghanistan-iran.pdf

706 Hossenzadeh, S.R., 1997. One hundred and twenty days winds of Sistan. Iran Iran. J Res Geogr. 46,
707 103–127.

708 Huffman, G., Adler, R., Bolvin, D., Gu, G., Nelkin, E., Bowman, K., Hong, Y., Stocker, E., Wolff, D.,

709 2007. The TRMM multi-satellite precipitation analysis: Quasi-global, multi-year, combined
710 sensor precipitation estimates at fine scales. J. Hydrometeorol. 8, 28–55.

711 ICANA, 2015. 25% migration of Sistan people due to drought [WWW Document]. URL
712 khabaronline.ir/news/587938 (accessed 8.25.20).

713 Iran Department of Environment (DOE), 2014. Determining the environmental flow needs of
714 Hamun wetlands.

715 Iran Ministry of Enegry (MoE), 2013. Update of Sistan River studies (hydrological report).

716 Iranian Consultative Assembly News Aagency (ICANA), 2012. “Hamoon” is the artery of Sistan
717 [WWW Document]. URL https://www.icana.ir/Fa/News/248571/%22-هامون%22شاهرگ-سیستان-
718 است (accessed 8.25.20).

719 Irannezhad, M., Haghighi, A.T., Chen, D., Kløve, B., 2015. Variability in dryness and wetness in
720 central Finland and the role of teleconnection patterns. Theor. Appl. Climatol. 122, 471–486.

721 Khazaei, B., Khatami, S., Alemohammad, S.H., Rashidi, L., Wu, C., Madani, K., Kalantari, Z., Destouni,
722 G., Aghakouchak, A., 2019. Climatic or regionally induced by humans? Tracing hydro-climatic
723 and land-use changes to better understand the Lake Urmia tragedy. J. Hydrol. 569, 203–217.

724 Kottek, M., Grieser, J., Beck, C., Rudolf, B., Rubel, F., 2006. World map of the Köppen-Geiger climate
725 classification updated. Meteorol. Zeitschrift 15, 259–263. https://doi.org/10.1127/0941-
726 2948/2006/0130

727 Lehner, B., Liermann, C.R., Revenga, C., Vörösmarty, C., Fekete, B., Crouzet, P., Döll, P., Endejan, M.,
728 Frenken, K., Magome, J., others, 2011. High-resolution mapping of the world’s reservoirs and

729 dams for sustainable river-flow management. Front. Ecol. Environ. 9, 494–502.

730 McKee, T.B., 1995. Drought monitoring with multiple time scales, in: Proceedings of 9th Conference
731 on Applied Climatology, Boston, 1995.

732 Meteorological Department of Sistan and Baluchestan, 2020. 120-day wind speed [WWW
733 Document]. URL https://sbmet.ir/ (accessed 6.3.21).

734 Mianabadi, A., Davary, K., Mianabadi, H., Karimi, P., 2020. International Environmental Conflict
735 Management in Transboundary River Basins. Water Resour. Manag. 34, 3445–3464.
736 https://doi.org/10.1007/s11269-020-02576-7

737 Mianabadi, H., Alioghli, S., Morid, S., 2021. Quantitative evaluation of ' No-harm ' rule in
738 international transboundary water law in the Helmand River basin. J. Hydrol. 599, 126368.
739 https://doi.org/10.1016/j.jhydrol.2021.126368

740 Micklin, P.P., 1988. Desiccation of the Aral Sea: a water management disaster in the Soviet Union.
741 Science (80-.). 241, 1170–1176.

742 Milly, P.C.D., Dunne, K.A., 2016. Potential evapotranspiration and continental drying. Nat. Clim.
743 Chang. 6, 946–949.

744 Ministry of Cooperatives Labour and Social Welfare Iran, 2017. Employment status of Sistan and
745 Baluchestan province.

746 Ministry of Energy (MoE), 2015. Report on water resources and consumption of Sistan and
747 Baluchestan province.

748 Ministry of Energy (MoE), 2014. Studies of the second phase of water supply in Sistan plain. Tehran.

749 Miri, A., Ahmadi, H., Ghanbari, A., Moghaddamnia, A., 2007. Dust storms impacts on air pollution
750 and public health under hot and dry climate. Int J Energy Env. 2, 101–105.

751 ModaresiRad, A., Kreitler, J., Abatzoglou, J.T., Fallon, K., Roche, K., Sadegh, M., 2022. Anthropogenic
752 stressors compound climate impacts on inland lake dynamics: The case of Hamun Lakes. Sci.
753 Total Environ. 154419.

754 Ouma, Y.O., Tateishi, R., 2006. A water index for rapid mapping of shoreline changes of five East
755 African Rift Valley lakes: an empirical analysis using Landsat TM and ETM+ data. Int. J. Remote
756 Sens. 27, 3153–3181. https://doi.org/10.1080/01431160500309934

757 Pekel, J.F., Cottam, A., Gorelick, N., Belward, A.S., 2016. High-resolution mapping of global surface
758 water and its long-term changes. Nature 540, 418–422. https://doi.org/10.1038/nature20584

759 Rahimi, R., Tavakol-Davani, H., Graves, C., Gomez, A., Valipour, M.F., 2020. Compound inundation
760 impacts of coastal climate change: Sea-level rise, groundwater rise, and coastal precipitation.
761 Water (Switzerland) 12, 1–16. https://doi.org/10.3390/w12102776

762 Rashki, A., Kaskaoutis, D.G., Goudie, A.S., Kahn, R.A., 2013. Dryness of ephemeral lakes and
763 consequences for dust activity: The case of the Hamoun drainage basin, Southeastern Iran. Sci.
764 Total Environ. 463–464, 552–564. https://doi.org/10.1016/j.scitotenv.2013.06.045

765 Rashki, A., Kaskaoutis, D.G., Rautenbach, C.J. d. W., Eriksson, P.G., Qiang, M., Gupta, P., 2012. Dust
766 storms and their horizontal dust loading in the Sistan region, Iran. Aeolian Res. 5, 51–62.
767 https://doi.org/10.1016/j.aeolia.2011.12.001

768 Rokni, K., Ahmad, A., Selamat, A., Hazini, S., 2014. Water Feature Extraction and Change Detection
769 Using Multitemporal Landsat Imagery 4173–4189. https://doi.org/10.3390/rs6054173

770 Rouse Jr, J.W., 1973. Monitoring the vernal advancement and retrogradation (green wave effect) of
771 natural vegetation.

772 Saemian, P., Hosseini-Moghari, S.-M., Fatehi, I., Shoarinezhad, V., Modiri, E., Tourian, M.J., Tang, Q.,
773 Nowak, W., Bárdossy, A., Sneeuw, N., 2021. Comprehensive evaluation of precipitation
774 datasets over Iran. J. Hydrol. 603, 127054. https://doi.org/10.1016/j.jhydrol.2021.127054

775 Schneider, U., Becker, A., Finger, P., Meyer-Christoffer, A., Rudolf, B., Ziese, M., 2011. Monthly land-
776 surface precipitation from rain-gauges built on GTS-based and historic data. Glob. Precip. Clim.
777 Cent.(GPCC), Dtsch. Wetterdienst, doi 10.

778 Sheffield, J., Wood, E.F., Roderick, M.L., 2012. Little change in global drought over the past 60 years.
779 Nature 491, 435–438. https://doi.org/10.1038/nature11575

780 Shukla, S., Wood, A.W., 2008. Use of a standardized runoff index for characterizing hydrologic
781 drought. Geophys. Res. Lett. 35.

782 Statistical Center of Iran, 2016. Results of the general population and housing census in 2016
783 [WWW Document]. URL https://www.amar.org.ir/english (accessed 11.26.20).

784 Tadono, T., Nagai, H., Ishida, H., Oda, F., Naito, S., Minakawa, K., Iwamoto, H., 2016. Generation of
785 the 30 M-mesh global digital surface model by ALOS PRISM. Int. Arch. Photogramm. Remote
786 Sens. Spat. Inf. Sci. 41.

787 The Convention on Wetlands, 1975. Ramsar Sites Information Service [WWW Document]. URL
788 https://rsis.ramsar.org/ (accessed 1.1.20).

789 Thom, H.C.S., 1966. Some methods of climatological analysis. WMO Tech. Note81.

790 Thomas, V., Varzi, M.M., 2015. A legal licence for an ecological disaster: the inadequacies of the
791 1973 Helmand/Hirmand water treaty for sustainable transboundary water resources
792 development. Int. J. Water Resour. Dev. 31, 499–518.

793 Torabi Haghighi, A., Sadegh, M., Behrooz-Koohenjani, S., Hekmatzadeh, A.A., Karimi, A., Kløve, B.,
794 2020. The mirage water concept and an index-based approach to quantify causes of
795 hydrological changes in semi-arid regions. Hydrol. Sci. J. 65, 311–324.

796 WHO, 2016. Global Health Observatory data repository [WWW Document]. World Heal. Organ. URL
797 https://apps.who.int/gho/data/view.main.AMBIENTCITY2016?lang=en (accessed 11.8.20).

798 Williams-Sether, T., 2008. Streamflow characteristics of streams in the Helmand Basin, Afghanistan.
799 US Department of the Interior, US Geological Survey.

800 Zaki, N.A., Haghighi, A.T., Rossi, P.M., Tourian, M.J., Bakhshaee, A., Kløve, B., 2020. Evaluating
801 impacts of irrigation and drought on river, groundwater and a terminal Wetland in the
802 Zayanderud Basin, Iran. Water (Switzerland) 12. https://doi.org/10.3390/W12051302

803 Zaki, N.A., Haghighi, A.T., Rossi, P.M., Xenarios, S., Kløve, B., 2018. An index-based approach to
804 assess thewater availability for irrigated agriculture in sub-Saharan Africa. Water (Switzerland)
805 10. https://doi.org/10.3390/w10070896

806